

DRAFT VERSION JANUARY 26, 2022
 Typeset using L^AT_EX preprint2 style in AASTeX631

Two gas giants transiting M dwarfs confirmed with HPF and NEID

CALEB I. CAÑAS ^{1, 2,*} SHUBHAM KANODIA ^{1, 2} CHAD F. BENDER ^{1, 3} SUVRATH MAHADEVAN ^{1, 2}
 GUÐMUNDUR STEFÁNSSON ^{4, †} WILLIAM D. COCHRAN ⁵ ANDREA S.J. LIN ^{1, 2}
 LUKE POWERS ^{1, 2} ANDREW MONSON ¹ ELIZABETH M. GREEN ³ BROCK A. PARKER ^{1, 6}
 TERA N. SWABY ^{1, 6} HENRY A. KOBULNICKY ^{1, 6} JOHN WISNIEWSKI ^{1, 7} ARVIND F. GUPTA ^{1, 2}
 MARK E. EVERETT ^{1, 8} SINCLAIRE JONES ^{1, 4} BENJAMIN ANJAKOS ^{1, 9} COREY BEARD ^{1, 10}
 CULLEN H. BLAKE ^{1, 11} SCOTT A. DIDDAMS ^{1, 12, 13} ZEHAO DONG (董泽浩) ^{1, 9}
 CONNOR FREDRICK ^{1, 14, 13} ELNAZ HAKEMIAMJAD ^{1, 9} LESLIE HEBB ^{1, 15}
 JESSICA E. LIBBY-ROBERTS ^{1, 2} SARAH E. LOGSDON ^{1, 8} MICHAEL W. McELWAIN ^{1, 16}
 ANDREW J. METCALF ^{1, 17, 12, 13} JOE P. NINAN ^{1, 18} JAYADEV RAJAGOPAL ^{1, 8}
 LAWRENCE W. RAMSEY ^{1, 2} PAUL ROBERTSON ^{1, 10} ARPITA ROY ^{1, 19, 20} JACOB RUHLE ^{1, 9}
 CHRISTIAN SCHWAB ^{1, 21} RYAN C. TERRIEN ^{1, 22} AND JASON T. WRIGHT ^{1, 2, 23}

¹Department of Astronomy & Astrophysics, The Pennsylvania State University, 525 Davey Laboratory, University Park, PA 16802, USA

²Center for Exoplanets and Habitable Worlds, The Pennsylvania State University, 525 Davey Laboratory, University Park, PA 16802, USA

³Steward Observatory, The University of Arizona, 933 N. Cherry Avenue, Tucson, AZ 85721, USA

⁴Department of Astrophysical Sciences, Princeton University, 4 Ivy Lane, Princeton, NJ 08540, USA

⁵McDonald Observatory and Center for Planetary Systems Habitability, The University of Texas at Austin, Austin, TX 78730, USA

⁶Department of Physics & Astronomy, University of Wyoming, Laramie, WY 82070, USA

⁷Homer L. Dodge Department of Physics and Astronomy, University of Oklahoma, 440 W. Brooks Street, Norman, OK 73019, USA

⁸NSF's National Optical-Infrared Astronomy Research Laboratory, 950 N. Cherry Ave., Tucson, AZ 85719, USA

⁹Department of Astronomy, The University of Arizona, 933 N. Cherry Avenue, Tucson, AZ 85721, USA

¹⁰Department of Physics & Astronomy, The University of California, Irvine, Irvine, CA 92697, USA

¹¹Department of Physics and Astronomy, University of Pennsylvania, 209 South 33rd Street, Philadelphia, PA 19104

¹²Time and Frequency Division, National Institute of Standards and Technology, 325 Broadway, Boulder, CO 80305, USA

¹³Department of Physics, University of Colorado, 2000 Colorado Avenue, Boulder, CO 80309, USA

¹⁴Associate of the National Institute of Standards and Technology, 325 Broadway, Boulder, CO 80305, USA

¹⁵Department of Physics, Hobart and William Smith Colleges, 300 Pulteney Street, Geneva, NY 14456, USA

¹⁶Exoplanets and Stellar Astrophysics Laboratory, NASA Goddard Space Flight Center, Greenbelt, MD 20771, USA

¹⁷Space Vehicles Directorate, Air Force Research Laboratory, 3550 Aberdeen Ave. SE, Kirtland AFB, NM 87117, USA

¹⁸Department of Astronomy and Astrophysics, Tata Institute of Fundamental Research, Homi Bhabha Road, Colaba, Mumbai 400005, India

¹⁹Space Telescope Science Institute, 3700 San Martin Drive, Baltimore, MD 21218, USA

²⁰Department of Physics and Astronomy, Johns Hopkins University, 3400 N Charles St, Baltimore, MD 21218, USA

²¹Department of Physics and Astronomy, Macquarie University, Balaclava Road, North Ryde, NSW 2109, Australia

²²Department of Physics and Astronomy, Carleton College, One North College Street, Northfield, MN 55057, USA

Corresponding author: Caleb I. Cañas

canas@psu.edu

²³Penn State Extraterrestrial Intelligence Center, 525 Davey Laboratory, The Pennsylvania State University, University Park, PA, 16802, USA

(Received January 24, 2022)

ABSTRACT

We confirm the planetary nature of two gas giants discovered by TESS. TOI-3714 ($V = 15.24$, $J = 11.74$) is an M2 dwarf hosting a hot Jupiter ($M_p = 0.70 \pm 0.03 M_J$ and $R_p = 1.01 \pm 0.03 R_J$) on an orbital period of 2.154849 ± 0.000001 days with a resolved white dwarf companion. TOI-3629 ($V = 14.63$, $J = 11.42$) is an M1 dwarf hosting a hot Jupiter ($M_p = 0.26 \pm 0.02 M_J$ and $R_p = 0.74 \pm 0.02 R_J$) on an orbital period of $3.936551^{+0.000005}_{-0.000006}$ days. We characterize both transiting companions using a combination of ground-based and space-based photometry, speckle imaging, and high-precision velocimetry from the Habitable-zone Planet Finder and the NEID spectrographs. These systems are amenable to additional characterization with transmission spectroscopy to probe atmospheric chemistry and, for TOI-3714, obliquity measurements to probe formation scenarios.

1. INTRODUCTION

Short-period ($P < 10$ days) Jupiter-sized ($R_p \geq 8 R_\oplus$) exoplanets, or hot Jupiters, are rare in the Galaxy. Results from radial velocity (RV) surveys (e.g., Cumming et al. 2008; Mayor et al. 2011; Wright et al. 2012), ground-based photometry surveys (e.g., Obermeier et al. 2016), and space-based surveys (Howard et al. 2012; Petigura et al. 2018; Zhou et al. 2019) have determined the occurrence rate for hot Jupiters orbiting Sun-like (FGK) dwarfs to be $\lesssim 1\%$. Despite that over 400 hot Jupiters have been detected orbiting Sun-like stars, there is no consensus as to the origin mechanisms required to create this population of exoplanets (see Dawson & Johnson 2018). Many hypotheses have been proposed to explain the origin of these planets, including star-planet interactions (e.g., Wu & Murray 2003; Petrovich 2015a), planet-planet interactions (e.g., Naoz et al. 2011), migration due to planet-disk interactions (e.g., Lin et al. 1996), high-eccentricity migration (e.g., Rasio & Ford 1996; Weiden-

schilling & Marzari 1996; Ford & Rasio 2008; Petrovich 2015b), and *in-situ* formation (e.g., Boley et al. 2016; Batygin et al. 2016).

The core accretion theory of formation predicts a low abundance of Jupiter-like planets orbiting M dwarfs (e.g., Laughlin et al. 2004; Ida & Lin 2005; Kennedy & Kenyon 2008), the most abundant type of star in the Galaxy (Henry et al. 2018). In the core accretion model, a gas giant planet forms from a runaway process resulting in the rapid accretion of gas onto a planetary core (e.g., Pollack et al. 1996; Ida & Lin 2004; Hubickyj et al. 2005). This model predicts a small number of gas giants orbiting M dwarfs, because the low surface density of an M dwarf protoplanetary disk would impede the formation of massive cores required for the onset of runaway gas accretion.

To date, RV surveys (e.g., Endl et al. 2006; Bonfils et al. 2013; Sabotta et al. 2021) and photometric surveys (Kovács et al. 2013; Obermeier et al. 2016) have been unable to confirm the theoretical prediction of a lower occurrence rate for gas giants orbiting low-mass dwarfs. As of this writing, there are six hot Jupiters known to transit M dwarfs: Kepler-45 b (Johnson et al.

* NASA Earth and Space Science Fellow

† Henry Norris Russell Fellow

2012), HATS-6 b (Hartman et al. 2015), NGTS-1 b (Bayliss et al. 2018), HATS-71 b (Bakos et al. 2020), HATS-74A b (Jordán et al. 2021), and HATS-75b (Jordán et al. 2021).

In this paper, we confirm the planetary nature of two gas giants transiting the M dwarfs TOI-3714 (TIC 155867025, Gaia EDR3 178924390478792320) and TOI-3629 (TIC 455784423, Gaia EDR3 2881820324294985856). We characterize each system using space and ground-based photometry, speckle imaging, and precision RVs obtained with the Habitable-zone Planet Finder (HPF; Mahadevan et al. 2012, 2014) and NEID (Schwab et al. 2016; Halverson et al. 2016) spectrographs. We derive stellar parameters for the host stars using our HPF spectra and use the RVs measured from both HPF and NEID to confirm each transiting companion is a hot Jupiter.

This paper is structured as follows: Section 2 presents the photometric, imaging, and spectroscopic observations used to characterize each system. The characterization of the host stars and the best estimates of the stellar parameters are described in Section 3. The modeling and analysis of the photometry and RVs are presented in Section 4. Section 5 provides further discussion of the nature of these planets and the feasibility for future study. We end with a summary of our key results in Section 6.

2. OBSERVATIONS

2.1. TESS

TESS (Ricker et al. 2015) observed TOI-3629 and TOI-3714 in long-cadence mode (30 min cadence) during Sector 17 (2019 October 7 through 2019 November 2) and Sector 19 (2019 November 27 through 2019 December 24), respectively. Similar to TOI-1899 (Cañas et al. 2020), we identified TIC-455784423.01 as a planetary candidate using a custom pipeline to search for transiting candidates orbiting M dwarfs in short and long-

cadence TESS data. Our pipeline uses the `lightkurve` package (Lightkurve Collaboration et al. 2018) to detrend the data with a Savitzky-Golay filter and uses the box least-squares algorithm (Kovács et al. 2002) to identify transit events. We detected one planet candidate with a depth of $\sim 1.5\%$ and a period of ~ 3.94 days. This event was subsequently identified and given the name TOI-3629.01 by the “quick-look pipeline” (QLP), developed by Huang et al. (2020a,b). This is one of the detections from the “faint star search”¹, an effort to extend the nominal search and vetting of TESS objects of interests to stars with a TESS magnitude of $T < 13.5$ (Kunimoto & Daylan 2021). TOI-3714 also has one planet candidate with a depth of $\sim 4.5\%$ and a period of ~ 2.15 days, which was only identified through the “faint star search”.

We extract the photometry from the TESS full-frame images using `eleanor` (Feinstein et al. 2019). `eleanor` uses the TESScut² service (Brasseur et al. 2019) to obtain a cut-out of 31×31 pixels of the calibrated full-frame images centered on each target. `eleanor` removes the background, corrects for systematics, and derives a light curve for various combinations of apertures when processing a target. The final light curve is the one which minimizes the combined differential photometric precision (CDPP) after the data are binned to 1 hour timescales. The CDPP was originally defined for Kepler and is formally the rms of the photometric noise on transit timescales (Jenkins et al. 2010). Minimizing the CDPP ensures that sharp features on relatively short timescales, such as transits, are preserved.

Panel (a) in Figures 1 and 2 presents the TESS full frame image cutouts and the apertures used to derive the light curves for each target. In

¹ <https://tess.mit.edu/qlp/>

² <https://mast.stsci.edu/tesscut/>

panel (b), a smaller 11x11 pixel subgrid of the TESS image and the light curve apertures are overplotted on images from the Zwicky Transient Facility (ZTF; Masci et al. 2019). For each target, the preferred aperture is a 2×1 rectangular aperture centered on the host star. To investigate the impact of background stars as a source of dilution, we searched the 11×11 TESS pixel grid centered on each target in Gaia EDR3 (Gaia Collaboration et al. 2021). Similar to Gandolfi et al. (2018), we use the Gaia G_{RP} bandpass as an approximation to the TESS bandpass. Gaia EDR3 reveals there are no bright ($\Delta G_{RP} < 4$) stellar companions in each aperture.

The TESS light curves used in this work are the CORR_FLUX values calculated by `eleanor`. The corrected flux removes signals correlated with position (x and y pixel position), measured background, and time in the simple aperture flux. Observations where the background is larger than the stellar flux (FLUX_BKG > CORR_FLUX) or with non-zero data quality flags (Table 28 in Tenenbaum & Jenkins 2018) are excluded from analysis. Figures 3 and 4 present all photometry, including the TESS light curve, analyzed in this work.

2.2. RBO 0.6m Telescope

We used the 0.6m telescope at the Red Buttes Observatory (RBO) in Wyoming (Kasper et al. 2016) to observe (i) TOI-3714 on the nights of 2021 August 16 and 2021 November 19 and (ii) TOI-3629 on the nights of 2021 September 26 and 2021 October 4. The 0.6m telescope is a f/8.43 Ritchey-Chrétien Cassegrain constructed by DFM Engineering, Inc. and equipped with an Apogee Alta F16M camera. The observations on 2021 October 4 of TOI-3629 were obtained in the Bessell V filter (Bessell 1990) while the other observations were obtained in the Bessell I filter. All observations used the 2×2 on-chip binning mode, which has a gain of 1.39 e⁻/ADU, a plate scale of 0.731"/pixel,

and a readout time of ~ 2.4 s. Each target was defocused moderately and observed using an exposure time of 240s.

The RBO light curves were derived using `AstroImageJ` (Collins et al. 2017). Following the methodology in Stefánsson et al. (2017), the estimated scintillation noise was included in the flux uncertainty. The final reductions used a photometric aperture radius of 10 pixels (7.3''), an inner sky radius of 20 pixels (14.6'') and an outer sky radius of 30 pixels (21.9'').

2.3. APO 3.5m Telescope

We used the 3.5m Astrophysical Research Consortium (ARC) Telescope Imaging Camera (ARCTIC; Huehnerhoff et al. 2016) on the ARC 3.5m Telescope at Apache Point Observatory (APO) to obtain a transit of TOI-3714 on the night of 2021 November 21. The observations were performed in the Sloan *i'* filter using an engineered diffuser (Stefánsson et al. 2017) with an exposure time of 45s. ARCTIC was operated in the quad and fast readout modes using the 4×4 on-chip binning mode to achieve a gain of 2 e⁻/ADU, a plate scale of 0.456''/pixel, and a readout time of 2.7 s. Similar to the RBO data, we processed the photometry using `AstroImageJ` and include the scintillation noise estimate in the flux uncertainty. The final reduction used a photometric aperture radius of 10 pixels (4.6''), an inner sky radius of 20 pixels (9.1'') and outer sky radius of 30 pixels (13.7'').

2.4. Kuiper 61" Telescope

We used the 61" (1.55m) Kuiper Telescope located on Mt. Bigelow, Arizona to observe TOI-3629 on the night of 2021 October 16. The Kuiper Telescope³ is equipped with a Mont4k SN3088 CCD, a 4096×4097 pixel sensor with a 9.7' \times 9.7' field of view. TOI-3629 was observed in the Harris R-band using a 30s expo-

³ <http://james.as.arizona.edu/~psmith/61inch/CCD/basicinfo.html>

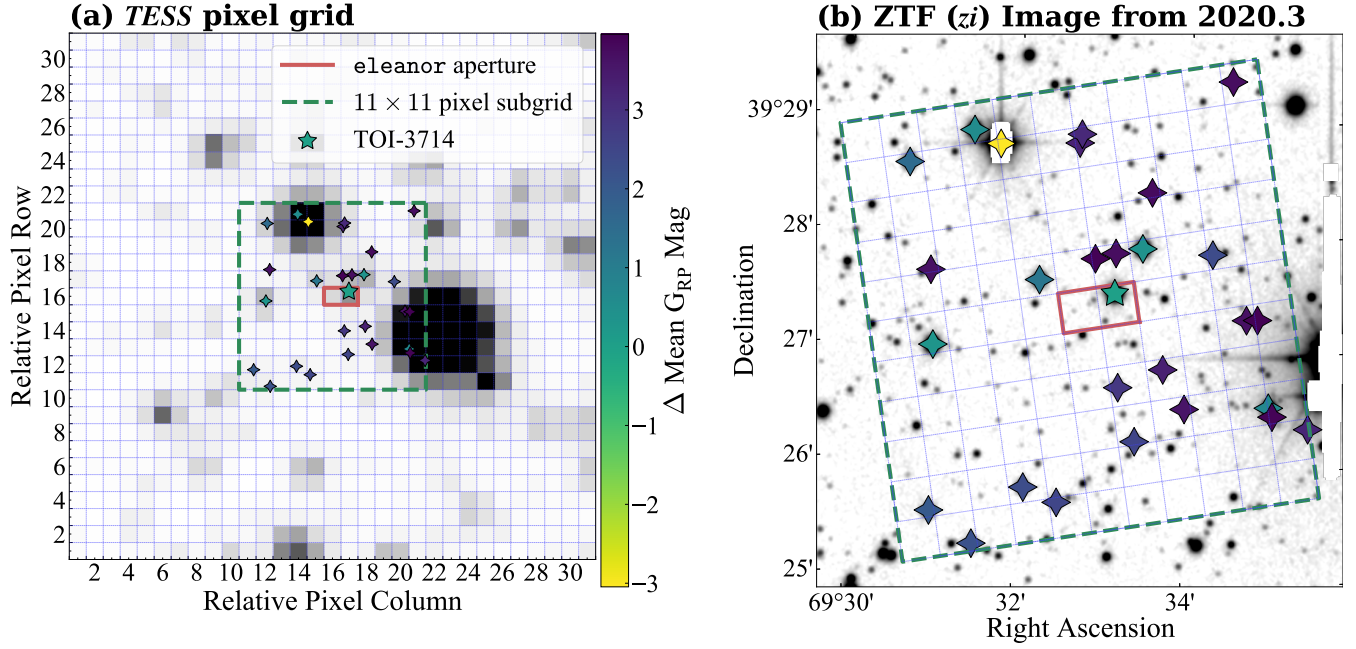


Figure 1. (a) The 31×31 TESS target pixel cutout centered around TOI-3714 (marked as a star). Stars identified in Gaia EDR3 with magnitudes $\Delta G_{\text{RP}} < 4$ are marked with diamond stars for reference. The dashed line denotes the TESS 11×11 pixel subgrid that is shown in (b). (b) Overlay of the TESS 11×11 pixel subgrid, TOI-3714, and other comparably bright stars on a ZTF *zi* image.

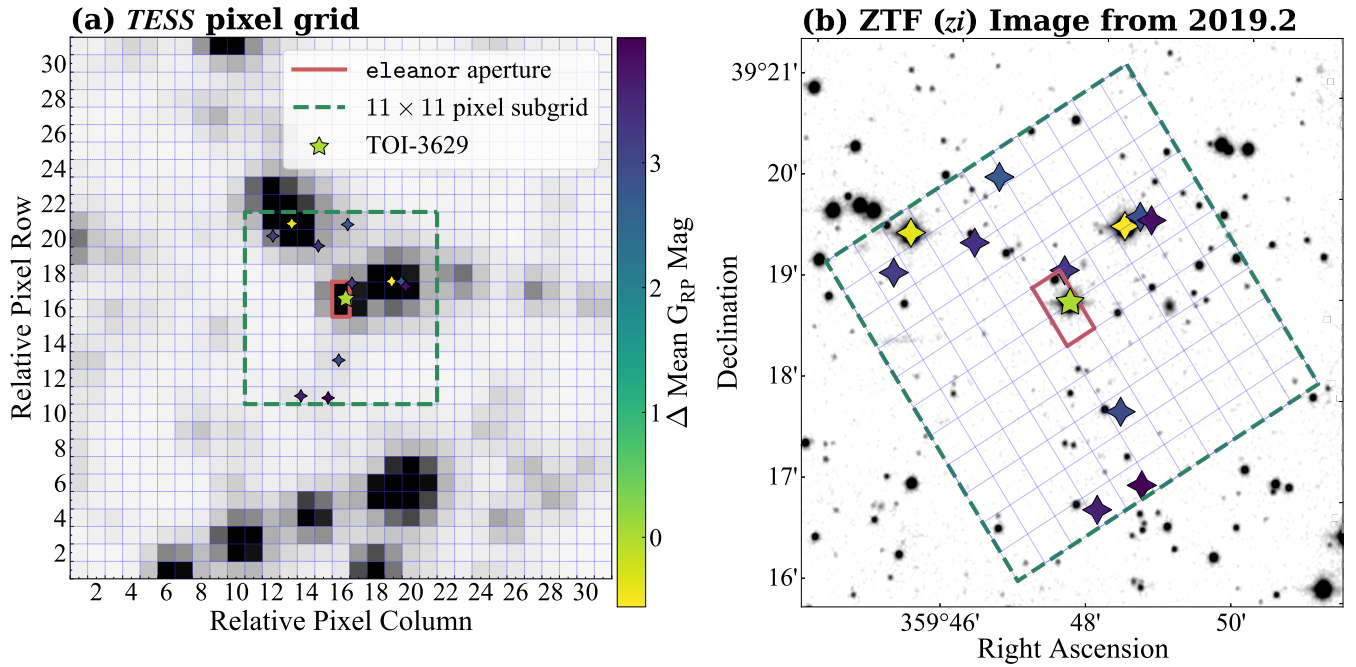


Figure 2. Identical to Figure 1 but for TOI-3629. (a) The 31×31 TESS target pixel cutout centered around TOI-3629 (marked as a star). Stars identified in Gaia EDR3 having magnitudes $\Delta G_{\text{RP}} < 4$ are marked with diamond stars. (b) Overlay of the TESS 11×11 pixel subgrid, TOI-3629, and other comparably bright stars on a ZTF *zi* image.

sure time with an average seeing of $\sim 1.7''$. The

pixels were binned in 3×3 mode to shorten

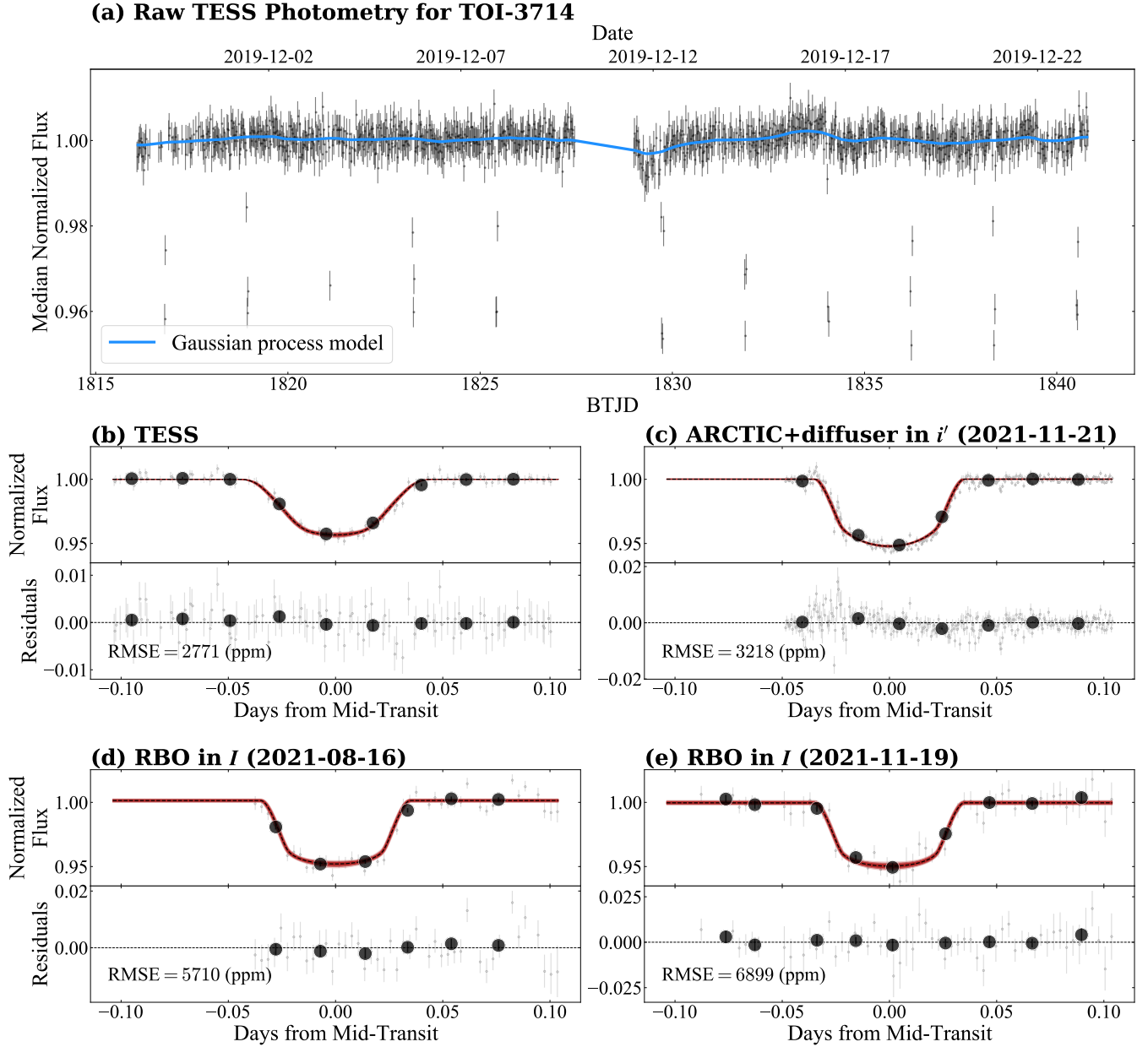


Figure 3. (a) The median normalized TESS light curve for TOI-3714 derived with `eleanor`. The solid blue line is the best-fitting Gaussian process model used to detrend the light curve. (b)–(e) are the light curves for TESS, ARCTIC, and RBO. In (b)–(e), the best-fitting model from the joint fit to the photometry and RVs is plotted as a dashed line while the shaded regions denote the 1 σ (darkest), 2 σ , and 3 σ (lightest) extent of the model posteriors. The large circles represent 30-minute bins of the data. The modeling of the photometry and RVs is described in detail in Section 4.

the readout time. This achieves a plate scale of 0.42''/pixel. Similar to the RBO data, we processed the photometry using `AstroImageJ` and include the scintillation noise estimate in the flux uncertainty. The final reduction used a photometric aperture radius of 8 pixels (3.6''),

an inner sky radius of 14 pixels (6.3'') and outer sky radius of 22 pixels (9.9'').

2.5. High-Contrast Imaging

TOI-3629 and TOI-3714 were observed on 2021 October 25 and 2021 December 21 respectively, using the speckle imaging instrument

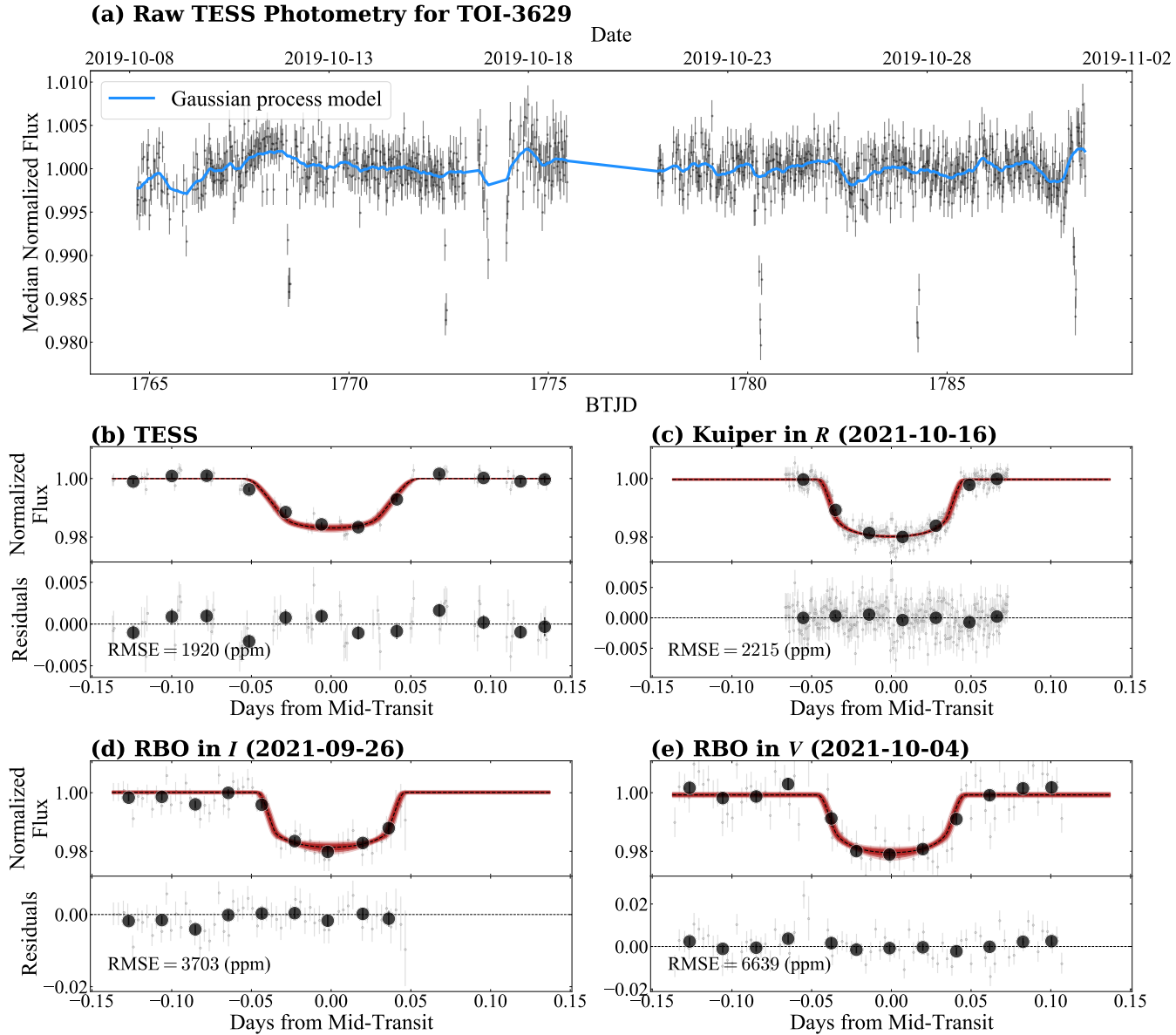


Figure 4. Identical to Figure 3, but for TOI-3629. **(a)** The median normalized TESS light curve for TOI-3629 derived with `eleanor` along with the best-fitting Gaussian process model. **(b)–(e)** are the light curves for the TESS, Kuiper, and RBO plotted with model posteriors (shaded regions) from the joint fit to the photometry and RVs. The large circles represent 30-minute bins of the data.

NESSI (Scott et al. 2018) on the WIYN 3.5m Telescope at Kitt Peak National Observatory (KPNO). Due to the faintness of these targets ($r' > 14$), the images were acquired in Sloan r' (TOI-3629 only) and z' instead of the narrower filters that NESSI traditionally uses. TOI-3714 was observed only in the Sloan z' filter because hardware issues during the observing run allowed for operations only with the redder filter.

The images in each filter were reconstructed following the procedures outlined in Howell et al. (2011).

TOI-3629 was also observed as part of the Robo-AO Kepler M dwarf multiplicity survey (Lamman et al. 2020) on 2016 October 19. The observations were performed using the Robo-AO laser adaptive optics system (Baranec et al. 2013, 2014) on the 2.1m telescope at KPNO

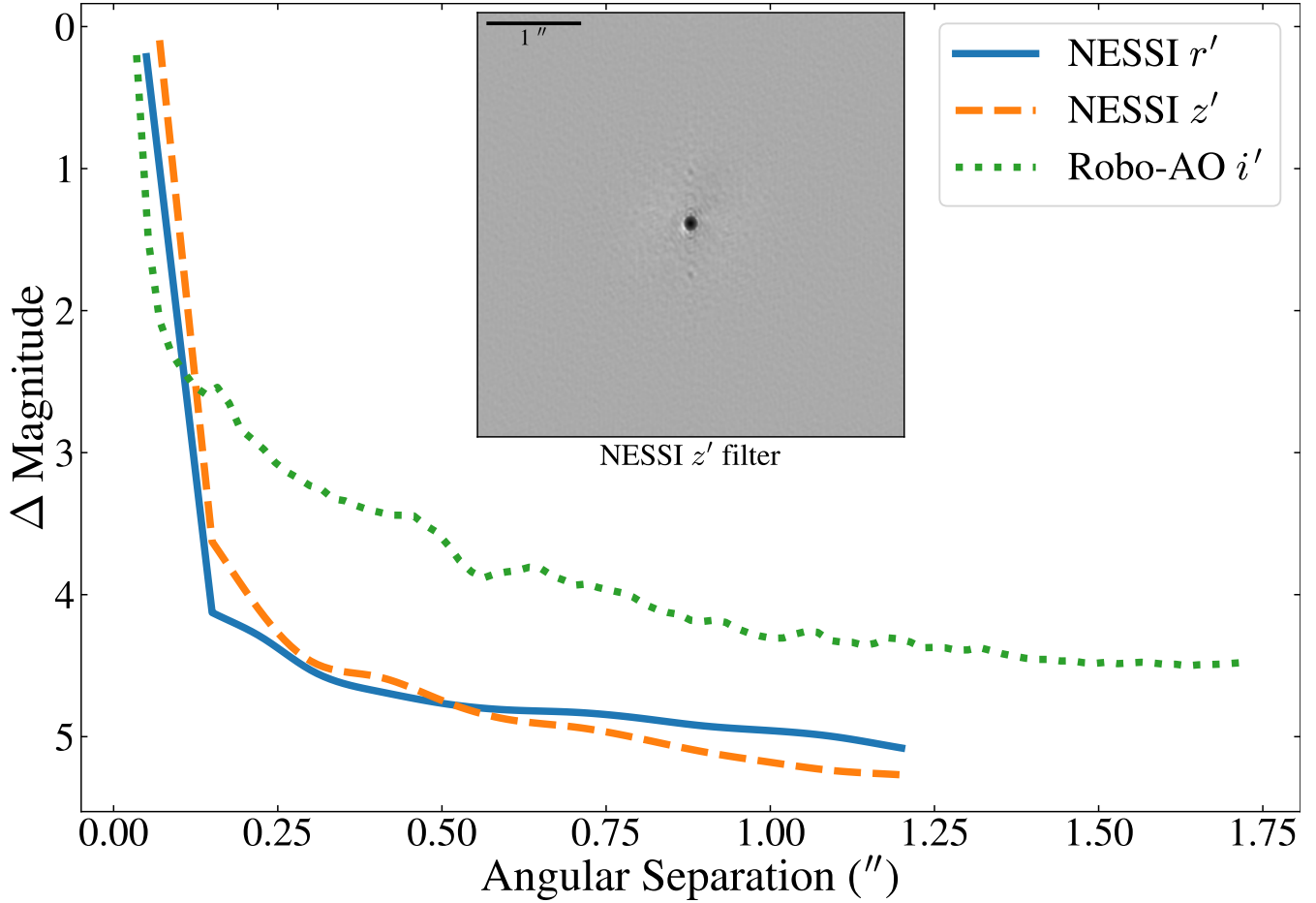


Figure 5. The 5σ contrast curves for TOI-3629 obtained from AO imaging using Robo-AO in the Sloan i' filter and speckle imaging with NESSI in the Sloan r' and z' filters. The data reveal no bright companions at separations of $0.2'' - 1.75''$ from TOI-3629. The inset is the $4.7'' \times 4.7''$ NESSI speckle image centered on TOI-3629 in the Sloan z' filter.

(Jensen-Clem et al. 2018) using a 1.85m circular aperture mask on the primary mirror. These observations were taken in the Sloan i' filter. Lamman et al. (2020) have made the Robo-AO contrast curve for TOI-3629 publicly available on ExoFOP-TESS⁴. The Robo-AO observation reveals no bright ($\Delta\text{mag} < 4$) stellar companions at separations of $0.75 - 1.75''$ from TOI-3629.

Figures 5 and 6 show the 5σ contrast curves for TOI-3629 and TOI-3714, respectively, along with an inset of the NESSI speckle image in the z' filter. Together, the NESSI and Robo-

AO data show there are no bright ($\Delta\text{mag} < 4$) companions and no significant source of dilution at separations of $0.2 - 1.2''$ from either target.

2.6. HPF Spectrograph

HPF is a high-resolution ($R \sim 55,000$), fiber-fed (Kanodia et al. 2018), temperature controlled (Stefánsson et al. 2016), near-infrared ($\lambda \sim 8080 - 12780 \text{ \AA}$) spectrograph located on the 10m Hobby-Eberly Telescope (HET) at McDonald Observatory in Texas (Mahadevan et al. 2012, 2014). Observations are executed in a queue by the HET resident astronomers (Shetrone et al. 2007). Between 2021 January 18 and 2022 January 14, we obtained 12 visits of TOI-3714 and 23 visits of TOI-3629. The

⁴ https://exofop.ipac.caltech.edu/tess/view_tag.php?tag=13940

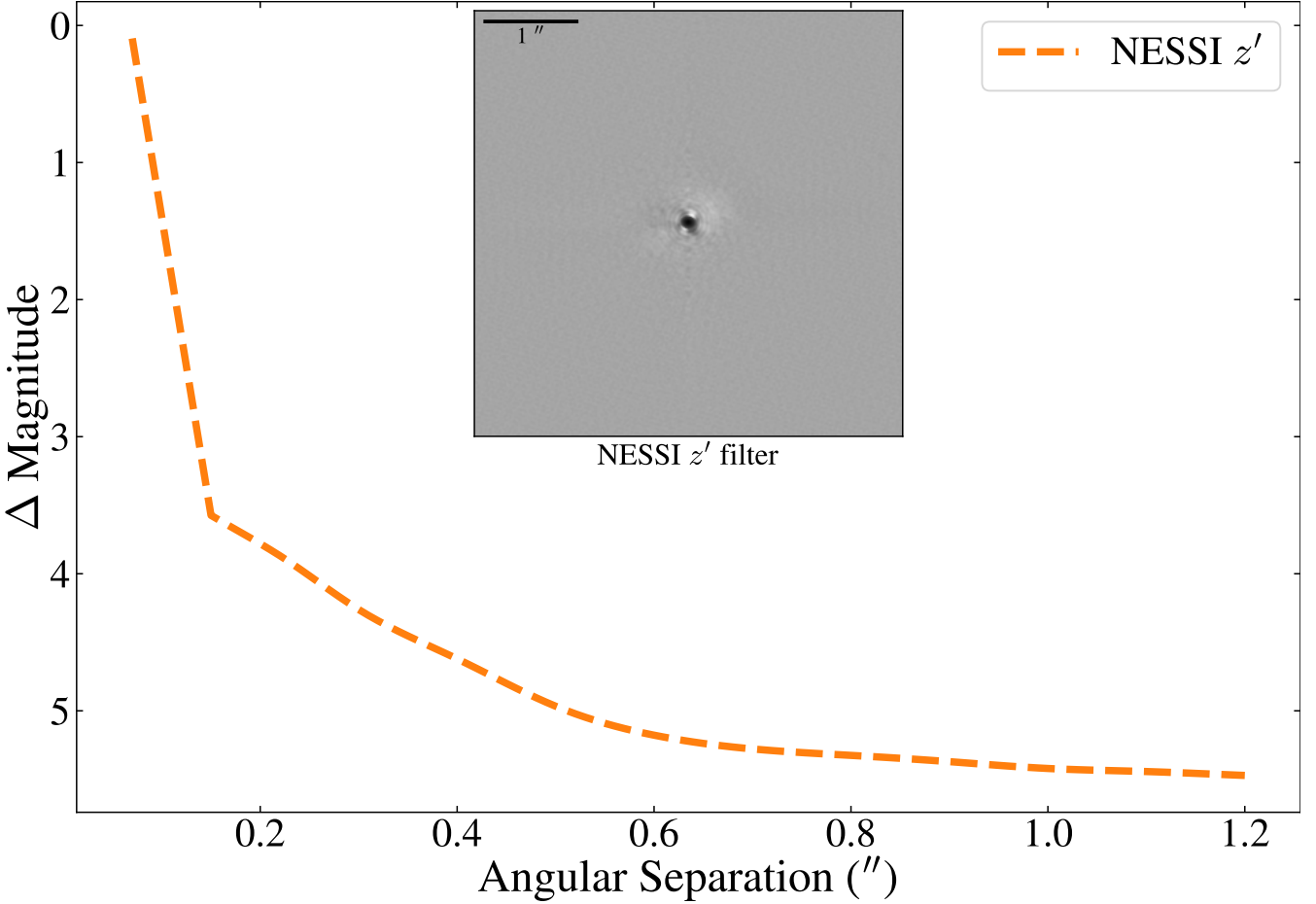


Figure 6. Similar to Figure 5 but for TOI-3714. The 5σ contrast curve for TOI-3714 obtained from speckle imaging using NESSI in the Sloan z' filter. The data reveal no bright companions at separations of $0.2'' - 1.75''$ from TOI-3714. The inset is the $4.7'' \times 4.7''$ NESSI speckle image centered on TOI-3714 in the Sloan z' filter.

median signal-to-noise ratios (S/N) per 1D extracted pixel at 1070nm are 44 and 54, respectively, for these targets.

The HxRGproc tool⁵ (Ninan et al. 2018) was used to process the raw HPF data and perform bias noise removal, nonlinearity correction, cosmic-ray correction, and slope/flux and variance image calculation. The one-dimensional spectra were extracted following the procedures in Ninan et al. (2018), Kaplan et al. (2019), and Metcalf et al. (2019). The wavelength solution and drift correction were extrapolated using laser frequency comb (LFC) frames obtained

from routine calibrations. This extrapolation enables wavelength calibration on the order of $< 30 \text{ cm s}^{-1}$ (see Appendix A in Stefánsson et al. 2020), a value which is much smaller than the RV uncertainty for our targets ($> 10 \text{ m s}^{-1}$).

The RVs were calculated using a modified version of the SpEctrum Radial Velocity AnaLyser code (SERVAL; Zechmeister et al. 2018) optimized for HPF RV extractions (see Metcalf et al. (2019) and Stefánsson et al. (2020) for details). SERVAL employs the template-matching technique to derive RVs (e.g., Anglada-Escudé & Butler 2012) and creates a master template from the observations to determine the Doppler shift by minimizing the χ^2 statistic. The master template is generated

⁵ <https://github.com/indiajoe/HxRGproc>

from all observed spectra after masking sky-emission lines and telluric regions identified using a synthetic telluric-line mask generated from `telfit` (Gullikson et al. 2014). The barycentric correction is calculated using `barycorpy`, a Pythonic implementation (Kanodia & Wright 2018) of the algorithms from Wright & Eastman (2014).

2.7. NEID Spectrograph

NEID is an environmentally stabilized (Stefánsson et al. 2016; Robertson et al. 2019), high-resolution ($R \sim 110,000$) spectrograph installed on the WIYN 3.5m telescope at KPNO in Arizona (Schwab et al. 2016). NEID features extended red wavelength coverage ($\lambda \sim 3800 - 9300 \text{ \AA}$) and a fiber-feed system similar to HPF (Kanodia et al. 2018). Between 2021 September 21 and 2022 January 8, we obtained 8 visits of TOI-3714 and 5 visits of TOI-3629. Observations were obtained in queue mode and NEID operated in high-resolution mode. The median S/N per 1D extracted pixel was 15 and 19, respectively, at 850nm.

The NEID data were reduced using the NEID Data Reduction Pipeline⁶ (DRP), and the Level-2 1D extracted spectra were retrieved from the NEID Archive⁷. Similar to HPF, to maximize the RV precision from the M dwarf spectra, we measured the RVs using a modified version of the SERVAL code (see Stefánsson et al. 2021). We extracted RVs with SERVAL using different segments of an order (inner 3000, 5000, or 7000 pixels) and different wavelength ranges (4950 – 8960 \AA or 5440 – 8960 \AA). The various combinations of pixel and wavelength ranges produced RVs that, when jointly modeled with photometry and HPF RVs, resulted in identical system parameters (within their 1σ uncer-

Table 1. RVs of TOI-3714 and TOI-3629.

BJD _{TDB}	RV (m s ⁻¹)	σ (m s ⁻¹)	S/N ^a	Exp. Time (s)	Instrument
TOI-3714:					
2459450.941268	-196	23	44	1890	HPF
2459451.948741	163	25	42	1890	HPF
2459452.941751	-183	22	47	1890	HPF
2459458.924675	15	25	41	1890	HPF
2459511.784103	60	23	44	1890	HPF
2459512.783671	29	23	46	1890	HPF
2459516.779359	209	26	40	1890	HPF
2459516.995256	64	20	50	1890	HPF
2459518.748189	119	30	35	1890	HPF
2459518.992056	135	23	44	1890	HPF
2459519.985625	-189	22	46	1890	HPF
2459571.844384	-103	29	34	1890	HPF
2459479.884140	71	12	15	1800	NEID
2459503.998300	27	15	11	1200	NEID
2459520.927772	77	11	15	1800	NEID
2459531.844720	58	10	16	1800	NEID
2459533.801149	89	9	18	1800	NEID
2459560.766674	-244	14	12	1800	NEID
2459586.625543	-239	11	15	1800	NEID
2459587.851477	91	20	9	1800	NEID
TOI-3629:					
2459232.579925	26	16	52	1890	HPF
2459233.576944	-24	18	48	1890	HPF
2459448.764453	28	13	66	1890	HPF
2459451.979492	1	18	49	1890	HPF
2459452.761162	5	15	59	1890	HPF
2459453.979751	-72	16	58	1890	HPF
2459455.739966	5	14	62	1890	HPF
2459457.974338	-42	13	64	1890	HPF
2459460.962548	-16	15	57	1890	HPF
2459461.955253	-91	18	48	1890	HPF
2459470.709176	-47	17	51	1890	HPF
2459471.707553	9	14	60	1890	HPF
2459475.919121	23	20	47	1890	HPF
2459477.918199	-72	18	50	1890	HPF
2459480.910306	-10	24	51	945	HPF
2459485.896427	-57	22	41	1890	HPF
2459499.627624	64	17	54	1890	HPF
2459507.814595	24	23	40	1890	HPF
2459516.581430	-20	15	59	1890	HPF
2459543.736198	11	15	60	1890	HPF
2459588.597139	-57	15	56	1890	HPF
2459592.597117	-48	15	60	1890	HPF
2459593.588844	44	16	54	1890	HPF
2459478.965087	-20	6	22	1800	NEID
2459479.794197	28	6	22	1800	NEID
2459528.888224	-34	14	11	1800	NEID
2459532.843589	-38	8	19	1800	NEID
2459546.840787	62	15	11	1800	NEID

^aThe HPF and NEID S/N are the median values per 1D extracted pixel at 1070nm and 850nm, respectively.

⁶ <https://neid.ipac.caltech.edu/docs/NEID-DRP/>

⁷ <https://neid.ipac.caltech.edu/>

tainty). The NEID RVs presented in this work were calculated using the wavelength range from $5440 - 8920 \text{ \AA}$ (order indices 61 – 104) and the inner most 3000 pixels of each order. This effectively uses the central blaze region of each order and limits the use of the lower S/N regions near the edge of each order. Table 1 reports the HPF and NEID RVs, the 1σ uncertainties, the S/N per pixel, and exposure times for TOI-3714 and TOI-3629. Figures 7 and 8 display the RVs for TOI-3714 and TOI-3629, respectively.

3. STELLAR PARAMETERS

3.1. Spectroscopic Parameters

The stellar effective temperature (T_e), surface gravity ($\log g_*$), and metallicity ([Fe/H]) were calculated using the `HPF-SpecMatch`⁸ package (Stefánsson et al. 2020), which derives stellar parameters using the empirical template matching methodology discussed in Yee et al. (2017). It identifies the best-matching spectra from a library of well-characterized stars using χ^2 minimization, creates a composite spectrum using a weighted, linear combination of the five best-matching library spectra, and derives the stellar properties using these weights. When searching for the best-matching library spectra, `HPF-SpecMatch` broadens the stellar templates using a linear limb darkening law. The reported uncertainty is the standard deviation of the residuals from a leave-one-out cross-validation procedure applied to the entire spectral library in the chosen spectral order.

The HPF spectral library contains 166 stars and spans the following parameter space: $2700 \text{ K} < T_e < 6000 \text{ K}$, $4.3 < \log g_* < 5.3$, and $-0.5 < [\text{Fe}/\text{H}] < 0.5$. The spectral matching is performed on HPF order index 5 (8534–8645 \AA) for both targets because this order has little to no telluric contamination. The resolution limit of HPF places a constraint of $v \sin i < 2 \text{ km s}^{-1}$

⁸ <https://gummiks.github.io/hpfspecmatch/>

for both TOI-3714 and TOI-3629. Table 2 presents the derived spectroscopic parameters with their uncertainties.

3.2. Spectral Energy Distribution Fitting

To derive model-dependent stellar parameters, we modeled the spectral energy distribution (SED) for each target using the EXOFASTv2 analysis package (Eastman et al. 2019). EXOFASTv2 calculates the bolometric corrections for the SED fit by linearly interpolating the precomputed bolometric corrections⁹ in $\log g_*$, T_e , [Fe/H], and A_V from the MIST model grids (Dotter 2016; Choi et al. 2016).

The SED fits use Gaussian priors on the (i) 2MASS J , H , K magnitudes, Sloan g' , r' , i' magnitudes and Johnson B , V magnitudes from Henden et al. (2018), and Wide-field Infrared Survey Explorer magnitudes (Wright et al. 2010); (ii) $\log g_*$, T_e , and [Fe/H] derived from `HPF-SpecMatch`, and (iii) the geometric distance calculated from Bailer-Jones et al. (2021) for each respective star. We apply an upper limit to the visual extinction based on estimates of Galactic dust (Green et al. 2019) calculated at the distance determined by Bailer-Jones et al. (2021). The $R_v = 3.1$ reddening law from Fitzpatrick (1999) is used to convert the extinction from Green et al. (2019) to a visual magnitude extinction. Table 2 contains the stellar priors and derived stellar parameters with their uncertainties. The model-dependent mass and radius are (i) $0.53 \pm 0.02 \text{ M}_\odot$ and $0.51 \pm 0.01 \text{ R}_\odot$ for TOI-3714 and (ii) $0.63 \pm 0.02 \text{ M}_\odot$ and $0.60^{+0.02}_{-0.01} \text{ R}_\odot$ for TOI-3629.

3.3. Spectral Classification

TOI-3714 was observed on 2012 January 11 while TOI-3629 was observed on 2018 November 11. The spectra were processed using the same pipeline as the other targets in this study. The spectra were extracted using the `ExoFitter` package (Bonomo et al. 2019) and the resulting spectra were compared to the MIST model grids (Dotter 2016; Choi et al. 2016) to determine the stellar parameters. The resulting stellar parameters are listed in Table 2.

⁹ http://waps.cfa.harvard.edu/MIST/model_grids.html#bolometric

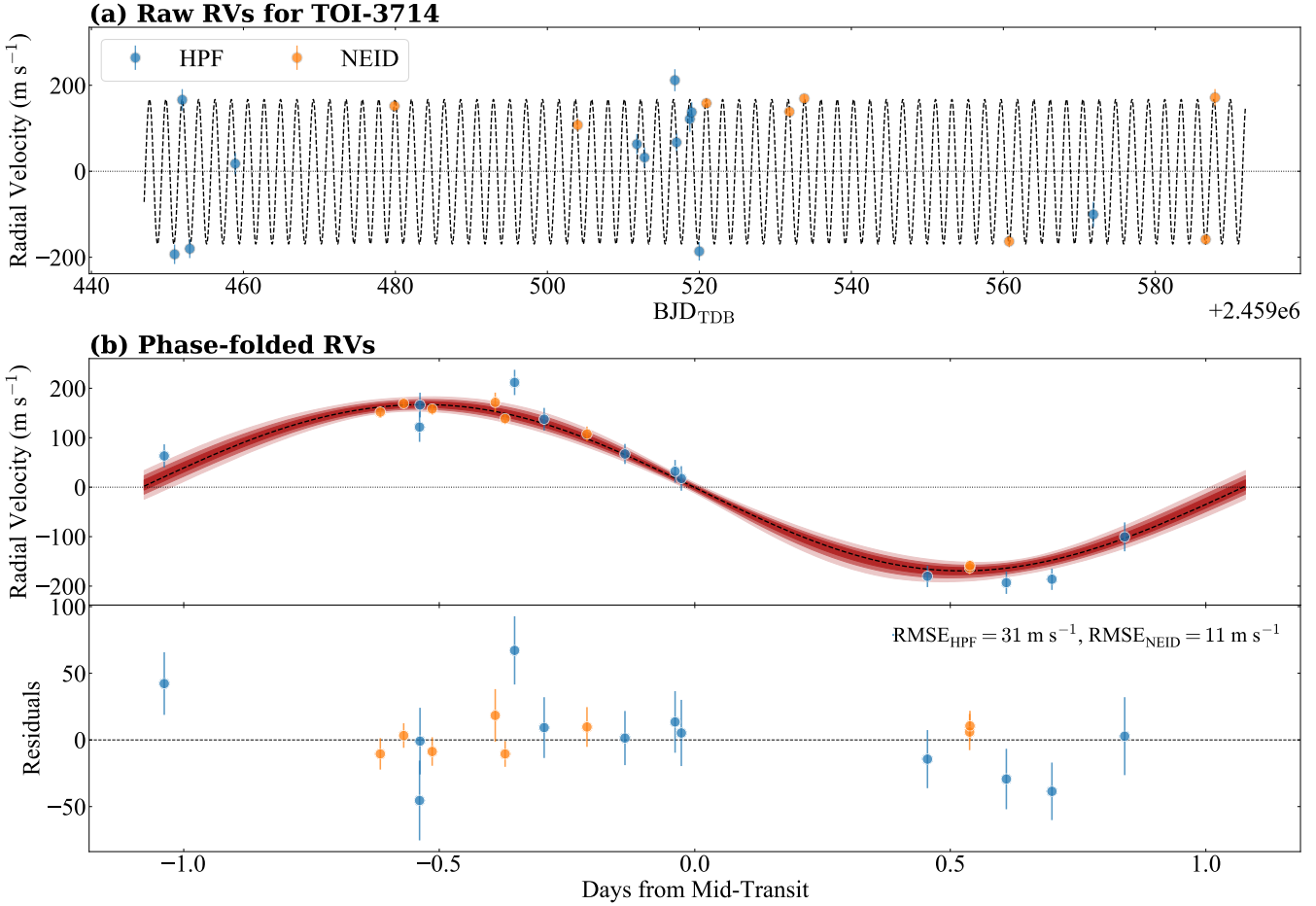


Figure 7. (a) shows the RVs for TOI-3714, after subtracting the instrumental offsets, derived with modified versions of SERVAL. (b) displays the phase-folded RVs plotted with model posteriors. For each panel, the dashed line is the best-fitting Keplerian model. The shaded regions denote the 1 σ (darkest), 2 σ , and 3 σ (lightest) extent of the model posteriors. The modeling is described in Section 4.

ber 3 by the Large Sky Area Multi-Object Fibre Spectroscopic Telescope (LAMOST) collaboration as part of its survey of the Galactic anti-center (Yuan et al. 2015; Xiang et al. 2017). LAMOST is a 4m telescope equipped with 4000 fibers distributed over a 5° FOV that is capable of acquiring spectra in the optical band (3700–9000Å) at a resolution $R \approx 1800$ with a limiting magnitude of SDSS $r' = 19$ mag (Cui et al. 2012). The data used in this work are from the public DR7v2.0¹⁰ release.

The LAMOST stellar classification pipeline uses stellar templates to identify molecular ab-

sorption features (e.g., CaH, TiO) that are typical for M-type stars (e.g., Zhong et al. 2015). To be classified as M dwarfs, targets must have (i) a mean S/N > 5, (ii) a best-matching template that is an M type, and (iii) the spectral indices of the absorption features must be located in the M-type stellar regime identified in Zhong et al. (2019) ($0 < \text{TiO5} < 1.2$ and $0.6 < \text{CaH2} + \text{CaH3} < 2.4$). LAMOST classifies TOI-3714 as an M2 dwarf and TOI-3629 as an M1 dwarf, which agrees with the derived parameters from HPF-SpecMatch in Section 3.1.

¹⁰ <http://dr7.lamost.org/>

3.4. Stellar Rotation Period

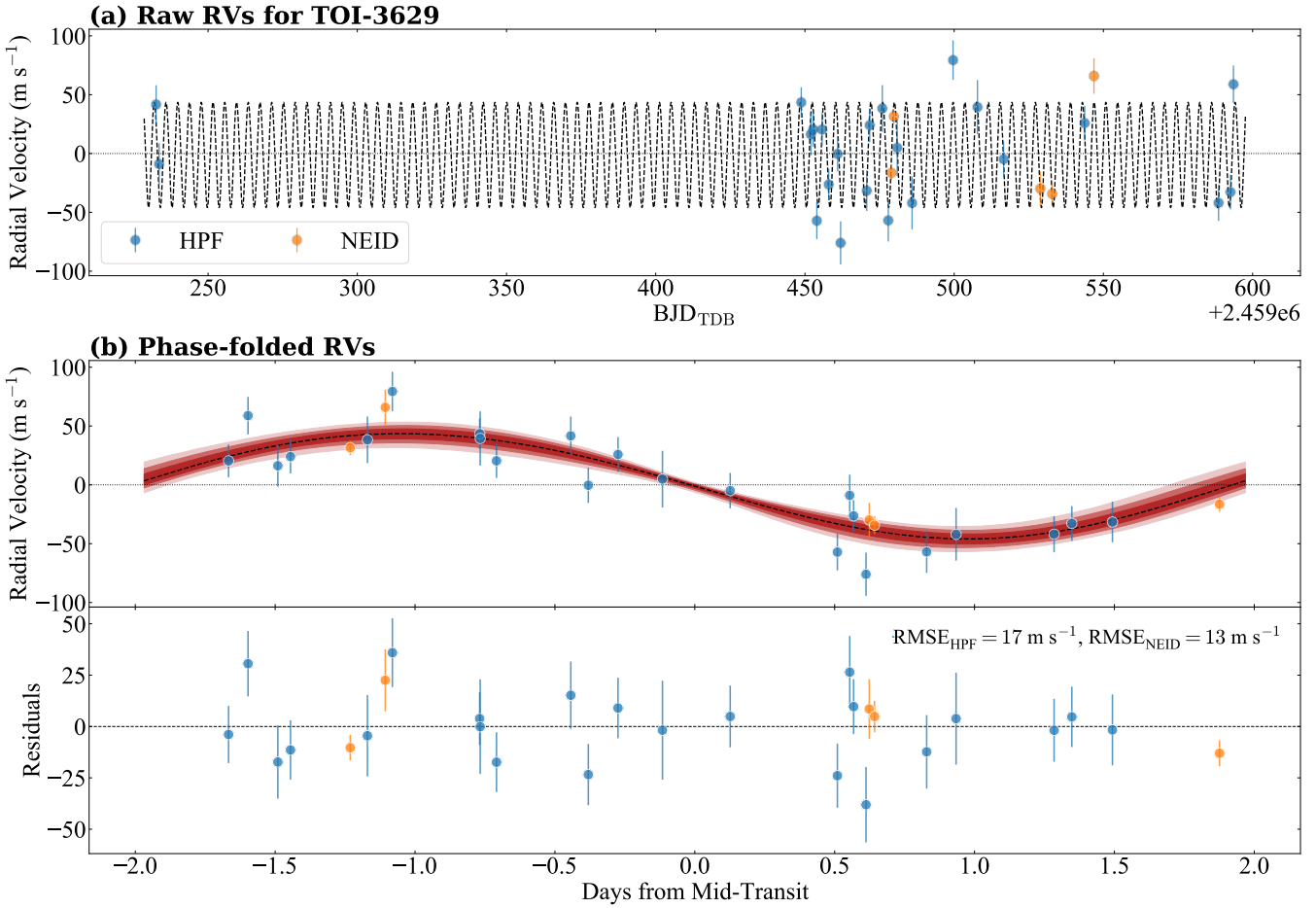


Figure 8. Identical to Figure 7, but for TOI-3629. **(a)** shows RVs for TOI-3629, after subtracting the instrumental offsets. **(b)** displays the phase-folded RVs plotted with model posteriors.

We used publicly available data from ZTF DR9¹¹ in the *zg* and *zr* filters to search for any signal caused by activity-induced photometric modulations in the target stars. This search for a rotation period used the generalized Lomb-Scargle (GLS) periodogram (Zechmeister & Kürster 2009) because it has been shown to successfully recover rotation periods in photometry (see VanderPlas 2018; Canto Martins et al. 2020; Reinhold & Hekker 2020). The GLS periodogram is based on Fourier decomposition and provides peaks in frequency space where the highest peak in the periodogram is associated with the period of the best fit sine wave that minimizes the χ^2 statistic. We use

the GLS¹² package to perform this analysis and only consider significant peaks where the false alarm probability, as calculated following Zechmeister & Kürster (2009), is below a threshold of 0.1%. A significant peak of ~ 23.6 days was found in the *zr* and *zg* photometry of TOI-3714. No significant peaks were seen in the ZTF photometry for TOI-3629.

To derive the rotation period and an estimate of its uncertainty, we modeled the ZTF photometry using the *juliet* analysis package (Espinoza et al. 2019), which performs the parameter estimation using the dynamic nested-sampling algorithm *dynesty* (Speagle 2020). The photometric model is a Gaussian process noise model using the approximate

¹¹ <https://irsa.ipac.caltech.edu/Missions/ztf.html>

¹² <https://github.com/mzechmeister/GLS>

Table 2. Summary of Stellar Parameters.

Parameter	Description	TOI-3714	TOI-3629	Reference
Main Identifiers:				
TIC	...	155867025	455784423	TIC
Gaia EDR3	...	178924390478792320	2881820324294985856	Gaia EDR3
Coordinates, Proper Motion, Distance, Maximum Extinction, and Spectral Type:				
α_{J2016}	Right Ascension (RA)	04:38:12.56	23:59:10.42	Gaia EDR3
δ_{J2016}	Declination (Dec)	39:27:28.77	39:18:51.32	Gaia EDR3
μ_α	Proper motion (RA, mas yr $^{-1}$)	19.83 \pm 0.03	185.71 \pm 0.01	Gaia EDR3
μ_δ	Proper motion (Dec, mas yr $^{-1}$)	-70.74 \pm 0.02	1.01 \pm 0.01	Gaia EDR3
l	Galactic longitude	163.30437	112.02292	Gaia EDR3
b	Galactic latitude	-5.02268	-22.44783	Gaia EDR3
d	Geometric distance (pc)	112.5 $^{+0.2}_{-0.4}$	129.7 \pm 0.3	Bailer-Jones
$A_{V,\text{max}}$	Maximum visual extinction	0.02	0.01	Green
Spectral Type	...	M2	M1	LAMOST
Broadband Photometric Magnitudes:				
B	Johnson B mag	16.8 \pm 0.2	16.1 \pm 0.1	APASS
V	Johnson V mag	15.24 \pm 0.09	14.63 \pm 0.05	APASS
g'	Sloan g' mag	15.9 \pm 0.1	15.33 \pm 0.04	APASS
r'	Sloan r' mag	14.73 \pm 0.09	14.08 \pm 0.05	APASS
i'	Sloan i' mag	13.66 \pm 0.09	13.12 \pm 0.07	APASS
J	J mag	11.74 \pm 0.02	11.42 \pm 0.03	2MASS
H	H mag	11.06 \pm 0.02	10.73 \pm 0.03	2MASS
K_s	K_s mag	10.85 \pm 0.02	10.55 \pm 0.02	2MASS
W1	WISE1 mag	10.72 \pm 0.02	10.48 \pm 0.02	WISE
W2	WISE2 mag	10.68 \pm 0.02	10.52 \pm 0.02	WISE
W3	WISE3 mag	10.5 \pm 0.1	10.38 \pm 0.07	WISE
Spectroscopic Parameters ^a :				
T_e	Effective temperature (K)	3660 \pm 90	3870 \pm 90	This work
$\log g_*$	Surface gravity (cgs)	4.75 \pm 0.05	4.67 \pm 0.05	This work
[Fe/H]	Metallicity (dex)	0.1 \pm 0.1	0.4 \pm 0.1	This work
$v \sin i^*$	Rotational broadening (km s $^{-1}$)	< 2	< 2	This work
Model-dependent Stellar SED and Isochrone Fit Parameters ^b :				
M_*	Mass (M_\odot)	0.53 \pm 0.02	0.63 \pm 0.02	This work
R_*	Radius (R_\odot)	0.51 \pm 0.01	0.60 $^{+0.02}_{-0.01}$	This work
ρ_*	Density (g cm $^{-3}$)	5.8 $^{+0.4}_{-0.3}$	4.0 \pm 0.2	This work
A_v	Visual extinction (mag)	0.011 \pm 0.007	0.005 \pm 0.003	This work
Age	Age (Gyrs)	0.7 – 5.1 ^c	7 $^{+5}_{-4}$	This work
Other Stellar Parameters:				
RV	Systemic RV (km s $^{-1}$)	36.4 \pm 0.2	-24.83 \pm 0.06	This work
P_{rot}	Stellar rotation period (days)	23.4 \pm 0.9	...	This work
U, V, W	Barycentric Galactic velocities (km s $^{-1}$)	-43.5 \pm 0.2, -23.9 \pm 0.1, -20.43 \pm 0.05	-91.9 \pm 0.2, -72.0 \pm 0.1, -13.06 \pm 0.06	This work
$(U, V, W)_{\text{LSR}}$	Galactic velocities w.r.t. LSR ^d (km s $^{-1}$)	-32.4 \pm 0.8, -11.7 \pm 0.5, -13.2 \pm 0.4	-80.8 \pm 0.8, -59.7 \pm 0.5, -5.8 \pm 0.4	This work

References—TIC (Stassun et al. 2019), Gaia EDR3 (Gaia Collaboration et al. 2021), Bailer-Jones (Bailer-Jones et al. 2021), Green (Green et al. 2019), LAMOST (Zhong et al. 2019), APASS (Henden et al. 2018), 2MASS (Cutri et al. 2003), WISE (Wright et al. 2010)

^a Derived with the `HFF-SpecMatch` package.

^b Derived with the `EXOFASTv2` package using MIST isochrones.

^c Age estimate from the rotation period and classification from Newton et al. (2016).

^d Calculated using the solar velocities from Schönrich et al. (2010).

quasi-periodic covariance function presented in Foreman-Mackey et al. (2017) of the form:

$$k(\tau) = \frac{B}{2+C} e^{-\tau/L} \left[\cos\left(\frac{2\pi\tau}{P_{\text{GP}}}\right) + (1+C) \right], \quad (1)$$

where τ is the scalar of choice (time), and B , C , L , and P_{GP} are the hyperparameters of the covariance function. B and C represent the weight of the exponential term with a decay constant of L (in days). P_{GP} determines the periodicity of the quasi-periodic oscillations, which is interpreted as the stellar rotation period. This kernel has been shown to reproduce the behavior of a more traditional quasi-periodic covariance function and has allowed for computationally ef-

ficient inference of stellar rotation periods even for large datasets that are not uniformly sampled (e.g., Angus et al. 2018).

The fit used a uniform prior on the Gaussian process period of 1 – 50 days. Figure 9 displays the phase-folded ZTF photometry and the posterior distribution on the rotation period. The measured rotation period is 23.4 \pm 0.9 days, which suggests that TOI-3714 has an age most likely between 0.7 – 5.1 Gyr after adopting the classification scheme of Newton et al. (2016). This age range is consistent with the rotation period and age relationship from Engle & Guinan (2018) and the values from our model-dependent SED fit. We are unable to place any

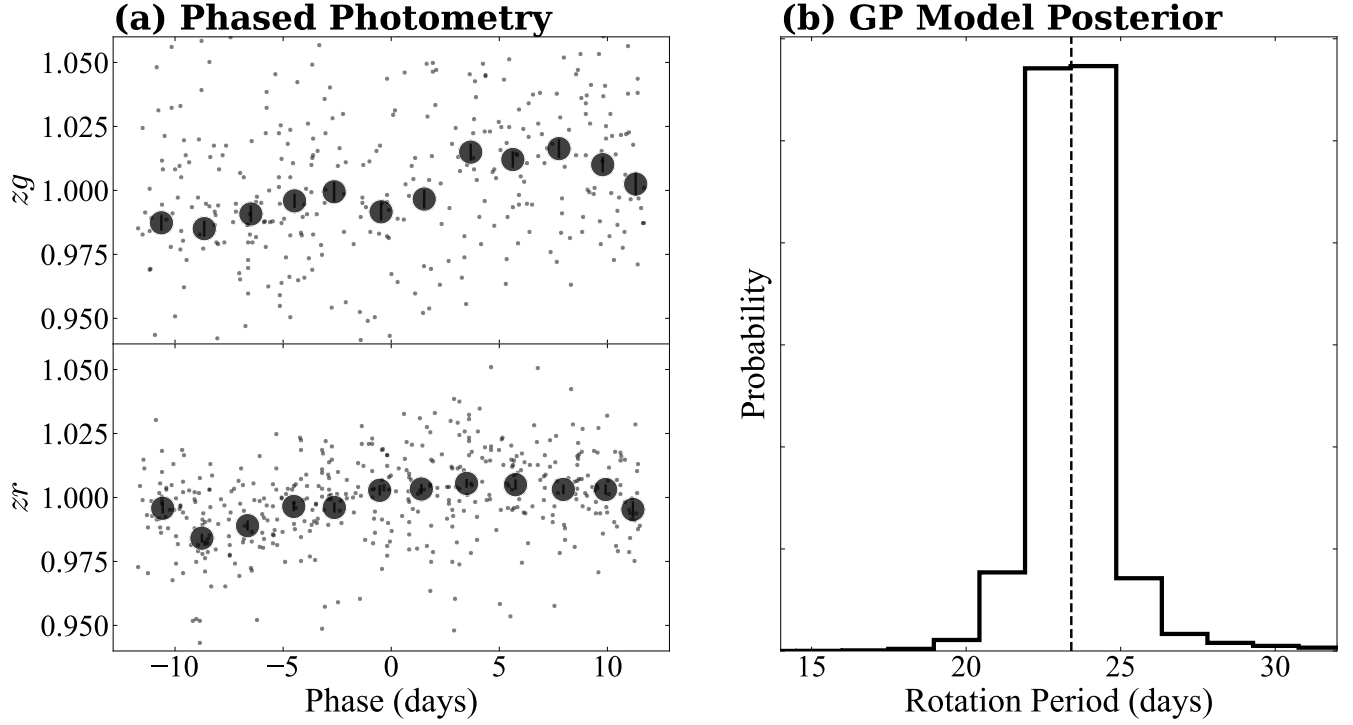


Figure 9. (a) presents the phased ground-based ZTF photometry for TOI-3714. The large black points represent 2-day bins of the phased photometry. (b) presents the posterior distribution of the rotation period from the Gaussian process model. The derived rotation period is 23.4 ± 0.9 days.

constraint on the rotation period of TOI-3629 due to the non-detection of a coherent signal in the ZTF photometry.

3.5. Galactic kinematics

The UVW velocities in the barycentric frame were derived with `galpy` (Bovy 2015) using the Gaia EDR3 proper motions and the systemic velocity derived from HPF. The values in Table 2 are in a right-handed coordinate system (Johnson & Soderblom 1987) where UVW are positive in the directions of the Galactic center, Galactic rotation, and the north Galactic pole, respectively. The UVW velocities in Table 2 are also provided with respect to the local standard of rest using the solar velocities and uncertainties from Schönrich et al. (2010). Using kinematic selection criteria from Bensby et al. (2003), both TOI-3629 and TOI-3714 are most probably members of the thin disk. The BANYAN Σ algorithm (Gagné et al. 2018), which uses sky positions, proper motions, par-

allax, and RVs to constrain cluster membership probabilities, classifies both TOI-3714 and TOI-3629 as field stars showing no associations with known young clusters.

4. PHOTOMETRIC AND RV MODELING

We use the `juliet` analysis package to jointly model the photometry and velocimetry and perform the parameter estimation using `dynesty`. `juliet` models the RVs with a standard Keplerian RV curve generated from the `radvel` (Fulton et al. 2018) package and models the light curves with a transit model generated from the `batman` package (Kreidberg 2015). The limb-darkening parameters are sampled from uniform priors following the parameterization presented in Kipping (2013a). For the long-cadence TESS photometry, the transit model utilizes the supersampling option in `batman` with exposure times of 30 minutes and a supersampling factor of 30. The photometric model also includes a dilution factor, D , for TESS representing the

ratio between the out-of-transit flux of the host star to that of all stars within the photometric aperture. We include this term for TESS data because `eleanor` does not correct for dilution from nearby stars despite the large apertures adopted (see Figures 1 and 2). Both the photometric and RV models include a simple white-noise model parameterized as a jitter term that is added in quadrature to the error bars of each data set. To account for correlated noise in the TESS light curves, each fit includes a Gaussian process noise model of the same form described in Section 3.4.

Tables 3 and 4 provide a summary of the priors used for the fit along with the inferred system parameters and the confidence intervals (16th – 84th percentile) for TOI-3714 and TOI-3629, respectively. Figures 3, 4, 7 and 8 display the model posteriors for each system. The modeling reveals that (i) TOI-3714.01 is a hot Jupiter ($M_2 = 0.70 \pm 0.03 M_J$ and $R_2 = 1.01 \pm 0.03 R_J$) orbiting its host star on a nearly circular orbit with a period of 2.154849 ± 0.000001 days and (ii) TOI-3629.01 is a hot Jupiter ($M_2 = 0.26 \pm 0.02 M_J$ and $R_2 = 0.74 \pm 0.02 R_J$) orbiting its host star on a nearly circular orbit with a period of $3.936551^{+0.000005}_{-0.000006}$ days.

5. DISCUSSION

5.1. Constraints on unresolved stellar companions

For both targets, the stellar density derived from the transit fit (see Seager & Mallén-Ornelas 2003; Winn 2010) in Section 4 is consistent with the value derived with an SED fit (Section 3). Following the methodology presented in Kanodia et al. (2020), we place limits on any spatially unresolved stellar companions

to our targets by quantifying the lack of flux from a secondary stellar object in the HPF spectra. The highest S/N spectrum for each target is parameterized as a linear combination of a primary M dwarf¹³ and a secondary stellar companion. The flux ratio between the secondary and primary star, F , is calculated as:

$$S_{\text{obs}} = A((1-x)S_{\text{primary}} + (x)S_{\text{secondary}}) \quad (2)$$

$$F = \frac{x}{1-x} \quad (3)$$

where S_{obs} is the observed spectrum, S_{primary} is the primary spectrum, $S_{\text{secondary}}$ represents the secondary spectrum, and A is the normalization constant. For a given primary and secondary template, we (i) shift the secondary spectrum in velocity space, (ii) add this shifted spectrum to the primary spectrum, and (iii) fit for the value of x that best fits the observed spectrum. We limit the secondary spectral type to M dwarfs earlier than M7 and to the orders where telluric absorption is minimal.

Figure 10 presents the results from HPF order index 17 spanning $10450 - 10580$ Å. We place a conservative upper limit for a secondary of flux ratio = 0.07 or $\Delta\text{mag} \simeq 2.9$ for both TOI-3714 and TOI-3629. As shown in Figure 10, there is no significant flux contamination at $|\Delta v| > 5 \text{ km s}^{-1}$. We perform this secondary light analysis for velocity offsets from $5 - 100 \text{ km s}^{-1}$, where the lower limit coincides with the spectral resolution of HPF ($\sim 5.5 \text{ km s}^{-1}$). The degeneracy between the primary and secondary spectra at velocity offsets $< 5 \text{ km s}^{-1}$ prevent any meaningful flux ratio constraints at those velocity offsets.

5.2. Constraints on unresolved bound companions

We use `thejoker` (Price-Whelan et al. 2017) to perform a rejection sampling analysis on the

¹³ GJ_205 and BD+29_2279 for TOI-3714 and TOI-3629, respectively, as identified by HPF-SpecMatch

Table 3. System Parameters for TOI-3714

Parameter	Units	Prior	Value			
Photometric Parameters						
Linear Limb-darkening Coefficient ^a	q_1	$\mathcal{U}(0, 1)$	$0.4^{+0.2}_{-0.1}$	0.5 ± 0.2	0.5 ± 0.2	0.4 ± 0.1
Quadratic Limb-darkening Coefficient ^a	q_2	$\mathcal{U}(0, 1)$	0.4 ± 0.2	$0.2^{+0.2}_{-0.1}$	$0.2^{+0.2}_{-0.1}$	0.5 ± 0.1
Photometric Jitter	σ_{phot} (ppm)	$\mathcal{J}(10^{-6}, 10^3)$	$0.007^{+1.765}_{-0.007}$	$0.003^{+1.431}_{-0.003}$	$0.03^{+11.3}_{-0.03}$	20^{+778}_{-20}
Dilution Factor	D	$\mathcal{U}(0, 2)$	0.87 ± 0.02
RV Parameters						
Systemic velocity	γ (m s ⁻¹)	$\mathcal{U}(-10^3, 10^3)$		-3 ± 7		-81 ± 6
RV Jitter	σ_{RV} (m s ⁻¹)	$\mathcal{J}(10^{-3}, 10^3)$		4^{+20}_{-4}		7^{+6}_{-3}
Orbital Parameters:						
Orbital Period	P (days)	$\mathcal{N}(2.15, 0.01)$			2.154849 ± 0.000001	
Time of Transit Center	T_C (BJD _{TDB})	$\mathcal{N}(2458840.51, 0.01)$			2458840.5093 ± 0.0004	
$\sqrt{e} \cos \omega$		$\mathcal{U}(-1, 1)$			0.0 ± 0.1	
$\sqrt{e} \sin \omega$		$\mathcal{U}(-1, 1)$			0.1 ± 0.1	
Semi-amplitude velocity	K (m s ⁻¹)	$\mathcal{J}(1, 10^3)$			169^{+6}_{-5}	
Scaled Radius	R_p/R_\star	$\mathcal{U}(0, 1)$			0.204 ± 0.003	
Impact Parameter	b	$\mathcal{U}(0, 1)$			$0.26^{+0.08}_{-0.1}$	
Scaled Semi-major Axis	a/R_\star	$\mathcal{J}(1, 100)$			$11.5^{+0.4}_{-0.5}$	
Gaussian Process Hyperparameters:						
B	Amplitude (ppm)	$\mathcal{J}(10^{-4}, 10^{12})$			$1.8^{+2.3}_{-0.7}$	
C	Additive Factor	$\mathcal{J}(10^{-3}, 10^3)$			1^{+50}_{-1}	
L	Length scale (days)	$\mathcal{J}(10^{-3}, 10^3)$			3^{+6}_{-2}	
P_{GP}	Period (days)	$\mathcal{J}(1.0, 100)$			11^{+30}_{-8}	
Derived Parameters:						
Eccentricity	e	...			$0.03^{+0.03}_{-0.02}$	
Argument of Periastron	ω (degrees)	...			100^{+61}_{-200}	
Orbital Inclination	i (degrees)	...			88.7 ± 0.5	
Transit Duration	T_{14} (hours)	...			$1.66^{+0.02}_{-0.01}$	
Mass	M_p (M _J)	...			0.70 ± 0.03	
Radius	R_p (R _J)	...			1.01 ± 0.03	
Surface Gravity	$\log g_p$ (cgs)	...			3.25 ± 0.04	
Density	ρ_p (g cm ⁻³)	...			0.85 ± 0.08	
Semi-major Axis	a (au)	...			0.027 ± 0.001	
Average Incident Flux	$\langle F \rangle$ (10 ⁸ erg s ⁻¹ cm ⁻²)	...			$0.74^{+0.06}_{-0.07}$	
Equilibrium Temperature ^b	T_{eq} (K)	...			750 ± 20	

^a Using the q_1 and q_2 parameterization from Kipping (2013a).

^b The planet is assumed to be a black body and we ignore heat redistribution.

residuals for the HPF RVs to constrain the existence of additional signals within the HPF RVs. This analysis used a log-uniform prior for the period (between $1 < P < 2000$ days), the Beta distribution from Kipping (2013b) as a prior for the eccentricity, and a uniform prior for the argument of pericenter and the orbital phase. For both TOI-3714 and TOI-3629, we analyzed $> 10^8$ (2^{28}) samples with the `joker` and had a total acceptance rate of $< 3\%$. The surviving samples place an upper limit on any low-inclination ($\sin i \sim 1$) companions of $M = 8.1$ M_J and

$M = 7.4$ M_J within 2.5 au for TOI-3714 and TOI-3629, respectively.

Gaia EDR3 provides an additional constraint on the presence of close-in, massive companions with the re-normalized unit weight error (RUWE) statistic. Lindegren et al. (2021) note that the RUWE, or the square root of the reduced χ^2 statistic that has been corrected for calibration errors, is sensitive to the photo-centric motions of unresolved objects. In systems with massive companions on orbital periods much shorter than the baseline of Gaia (34 months for EDR3), the astrometric motion

Table 4. System Parameters for TOI-3629

Parameter	Units	Prior	Value					
Photometric Parameters			TESS	RBO (09-26)	RBO (10-04)	Kuiper		
Linear Limb-darkening Coefficient ^a	q_1	$\mathcal{U}(0, 1)$	0.4 ± 0.2	$0.3^{+0.2}_{-0.1}$	$0.6^{+0.2}_{-0.3}$	0.7 ± 0.2		
Quadratic Limb-darkening Coefficient ^a	q_2	$\mathcal{U}(0, 1)$	$0.3^{+0.3}_{-0.2}$	0.5 ± 0.3	0.3 ± 0.2	0.21 ± 0.09		
Photometric Jitter	σ_{phot} (ppm)	$\mathcal{J}(10^{-6}, 10^3)$	$0.03^{+423.61}_{-0.03}$	$0.001^{+0.442}_{-0.001}$	$0.03^{+16.45}_{-0.03}$	10^{+421}_{-10}		
Dilution Factor	D	$\mathcal{U}(0, 2)$	0.90 ± 0.04		
RV Parameters			HPF		NEID			
Systemic velocity	γ (m s ⁻¹)	$\mathcal{U}(-10^3, 10^3)$	-15 ± 3		-4^{+10}_{-8}			
RV Jitter	σ_{RV} (m s ⁻¹)	$\mathcal{J}(10^{-3}, 10^3)$	5^{+5}_{-3}		16^{+10}_{-7}			
Orbital Parameters:								
Orbital Period	P (days)	$\mathcal{N}(3.94, 0.01)$	$3.936551^{+0.000005}_{-0.000006}$					
Time of Transit Center	T_C (BJD _{TDB})	$\mathcal{N}(2458784.26, 0.01)$	2458784.256 ± 0.001					
$\sqrt{e} \cos \omega$		$\mathcal{U}(-1, 1)$	-0.1 ± 0.1					
$\sqrt{e} \sin \omega$		$\mathcal{U}(-1, 1)$	$-0.1^{+0.2}_{-0.1}$					
Semi-amplitude velocity	K (m s ⁻¹)	$\mathcal{J}(1, 10^3)$	45 ± 4					
Scaled Radius	R_p/R_\star	$\mathcal{U}(0, 1)$	0.126 ± 0.002					
Impact Parameter	b	$\mathcal{U}(0, 1)$	0.2 ± 0.1					
Scaled Semi-major Axis	a/R_\star	$\mathcal{J}(1, 100)$	15.4 ± 0.8					
Gaussian Process Hyperparameters:								
B	Amplitude (ppm)	$\mathcal{J}(10^{-4}, 10^{12})$	$1.8^{+1.5}_{-0.5}$					
C	Additive Factor	$\mathcal{J}(10^{-3}, 10^3)$	3^{+80}_{-3}					
L	Length scale (days)	$\mathcal{J}(10^{-3}, 10^3)$	$0.8^{+1.6}_{-0.4}$					
P_{GP}	Period (days)	$\mathcal{J}(1.0, 100)$	9^{+37}_{-8}					
Derived Parameters:								
Eccentricity	e	...	$0.05^{+0.05}_{-0.04}$					
Argument of Periastron	ω (degrees)	...	-110^{+200}_{-40}					
Orbital Inclination	i (degrees)	...	89.1 ± 0.5					
Transit Duration	T_{14} (hours)	...	2.20 ± 0.03					
Mass	M_p (M _J)	...	0.26 ± 0.02					
Radius	R_p (R _J)	...	0.74 ± 0.02					
Surface Gravity	$\log g_p$ (cgs)	...	$3.09^{+0.06}_{-0.07}$					
Density	ρ_p (g cm ⁻³)	...	0.8 ± 0.1					
Semi-major Axis	a (au)	...	0.043 ± 0.002					
Average Incident Flux	$\langle F \rangle$ (10 ⁸ erg s ⁻¹ cm ⁻²)	...	0.53 ± 0.06					
Equilibrium Temperature ^b	T_{eq} (K)	...	690 ± 20					

^a Using the q_1 and q_2 parameterization from Kipping (2013a).

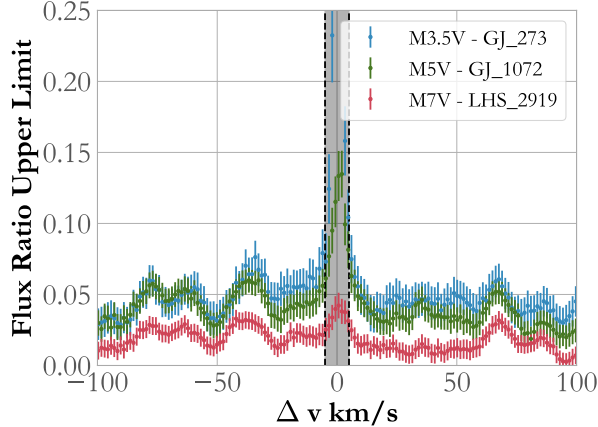
^b The planet is assumed to be a black body and we ignore heat redistribution.

of the primary star around the center of mass may appear as noise when adopting a single-star astrometric solution (e.g., Kervella et al. 2019; Kiefer et al. 2019). RUWE $\gtrsim 1.4$ is a threshold that correlates with the existence of an unresolved stellar companion in recent studies of stellar binaries (e.g., Belokurov et al. 2020; Penoyre et al. 2020; Gandhi et al. 2020; Stassun & Torres 2021). With RUWE values of 1.15 and 1.05, Gaia EDR3 suggests TOI-3714 and TOI-3629 do not have massive stellar companions on short-periods. Instead, these systems

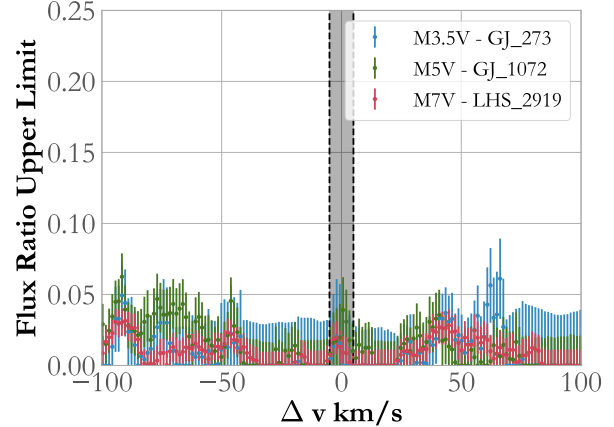
are in agreement with a single-star astrometric solution.

5.3. Constraints on resolved bound companions

We also use results from Gaia EDR3 to determine if either star has a wide separation stellar companion. El-Badry et al. (2021) provide a list of spatially resolved binary stars from an analysis of proper motions. TOI-3629 is not contained in the catalog but TOI-3714 is identified as having a white dwarf stellar companion, Gaia EDR3 178924390476838784 (TIC 662037581). Systems in El-Badry et al. (2021) are flagged as



(a) Flux ratio upper limits for TOI-3714.



(b) Flux ratio upper limits for TOI-3629.

Figure 10. Flux upper limits placed on the flux ratio of a secondary companion to a template spectrum as a function of Δv , obtained by fitting the wavelength region spanning $\sim 10450 - 10580 \text{ \AA}$ (HPF order index 17). We include the 1σ error bars, and shade the region corresponding to $\pm 5 \text{ km s}^{-1}$. We place a conservative upper limit on the flux ratio of 0.07 for an unresolved stellar companion at separations $|\Delta v| > 5 \text{ km s}^{-1}$.

having a white dwarf companion based on the location of the companion on the Gaia color-absolute magnitude diagram (El-Badry & Rix 2018). This object has a negligible probability ($\sim 0.0006\%$) of being the chance alignment of a background source with spurious parallax and proper motion measurements. The WD companion TIC 662037581 is located at a projected distance of $2.67''$ or a projected separation of 302 au from TOI-3714. This companion is outside both the HPF fiber ($\sim 1.7''$ on-sky; Kanodia et al. 2018) and the NEID HR fiber ($\sim 0.9''$ on-sky; Schwab et al. 2016).

To estimate the physical parameters of the white dwarf, we used the `WD_models`¹⁴ package from Cheng et al. (2019) to derive a photometric age and mass from its location (Figure 11) on the Gaia color-magnitude diagram (data from Gentile Fusillo et al. 2021). We assumed the atmosphere was composed of hydrogen and adopted the cooling models of Bédard et al. (2020). The estimated mass for the white dwarf companion is $M_{WD} \sim 1.07 \text{ M}_\odot$ with a cooling age of ~ 2.4 Gyr. The MIST semi-empirical

white dwarf initial-final mass relationship from Cummings et al. (2018) suggests the progenitor star had a mass between $4.5 - 6.8 \text{ M}_\odot$. Stars in this mass range have typical lifetimes (pre-main sequence through post-asymptotic giant branch) of < 0.1 Gyrs (Dotter 2016; Choi et al. 2016). Assuming this object is coeval with TOI-3714, the combined progenitor lifetime and white dwarf cooling age is consistent with the age range estimated from the rotation period in Section 3.4.

Approximately half of all hot Jupiter systems are known to have resolved stellar companions between separations of $50 - 2000$ au (e.g., Wang et al. 2014; Knutson et al. 2014; Ngo et al. 2015, 2016; Marzari & Thebault 2019; Fontanive & Bardalez Gagliuffi 2021) but only three other systems (see Veras 2016) are known to have a distant white dwarf companion: GJ 86 (Queloz et al. 2000; Mugrauer & Neuhäuser 2005; Farihi et al. 2013), η Ret (Butler et al. 2006; Farihi et al. 2011), and HD 147513 (see Appendix B in Desidera & Barbieri 2007). The existence of a distant stellar companion has been proposed as one mechanism to form hot Jupiters via a combination of secular interactions with the stel-

¹⁴ https://github.com/SihaoCheng/WD_models

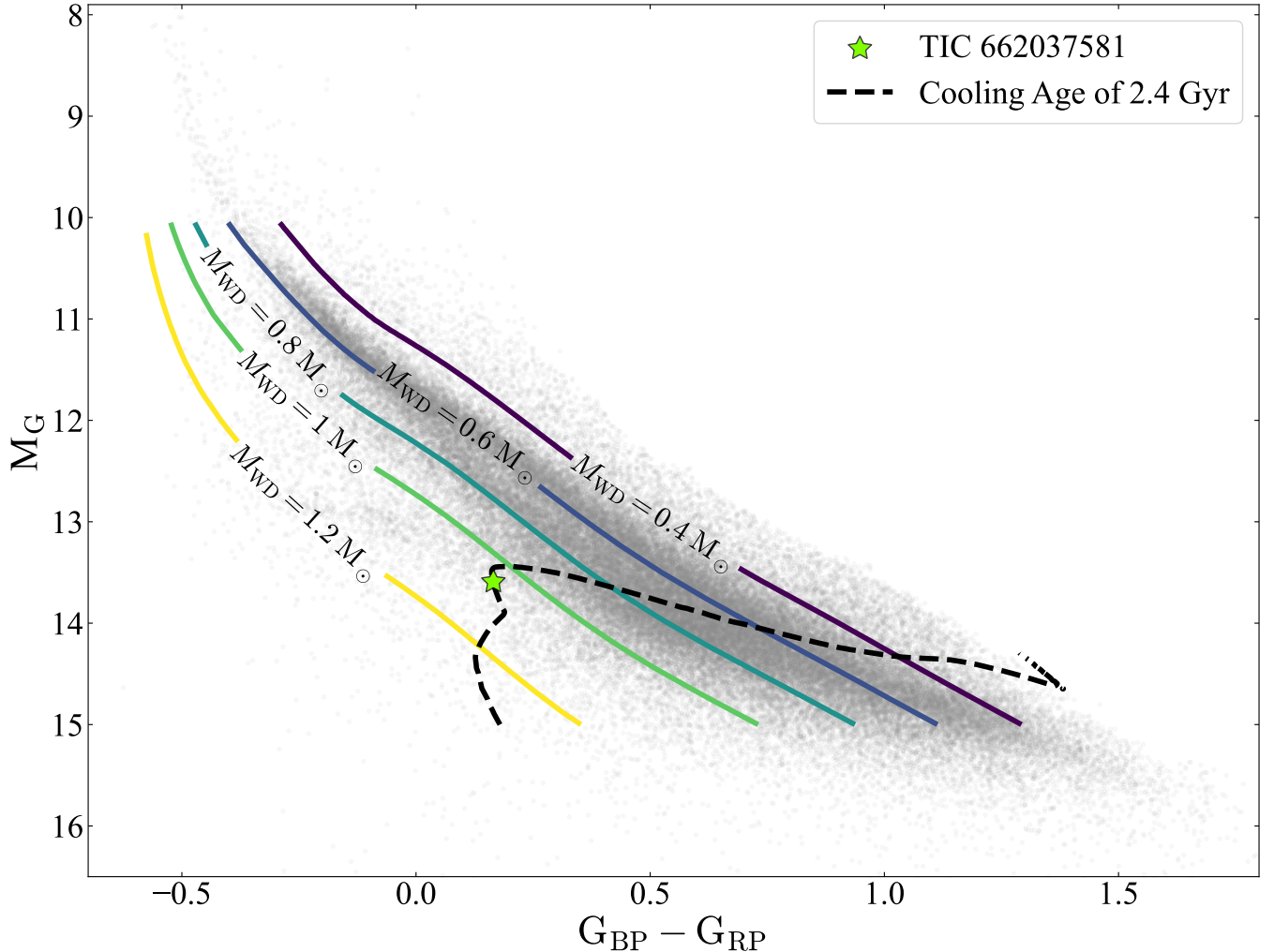


Figure 11. The position of TIC 662037581, the white dwarf companion to TOI-3714, on the color-magnitude diagram for the white dwarfs identified in Gaia EDR3 by Gentile Fusillo et al. (2021). Contours for fixed white dwarf masses from Bédard et al. (2020) are plotted for reference. The best-matching cooling track from the models is shown with a dashed line.

lar companion and tidal friction (e.g., Fabrycky & Tremaine 2007; Anderson et al. 2016; Vick et al. 2019). Ngo et al. (2016) note that most hot Jupiters with distant stellar companions are too separated to form via this mechanism.

If the TOI-3714 system was initially a wide binary with an initial progenitor separation ~ 302 au, the timescale for the Kozai cycles (Equation 7 from Kiseleva et al. 1998) would be ~ 2.8 Gyr. This timescale is comparable to the age of the system and too long to effectively perturb a gas giant. The separation between the progenitor star and TOI-3714 could not have been too small, as a stellar binary with an initial separa-

tion $a \lesssim 10$ au may interact when the primary star evolves off the main sequence and common envelope effects would subsequently shrink the orbit (see Paczyński 1971; Paczynski 1976; Ivanova et al. 2013). Instead, the progenitor star could have been on a smaller orbit of tens of au and the onset of mass loss could have caused the orbit to expand (see Nordhaus et al. 2010; Nordhaus & Spiegel 2013) to the observed separation. For example, at separations of 30 au, the Kozai timescale approaches ~ 3 Myr and it may be possible the white dwarf progenitor was close enough to perturb a nascent gas giant and far enough from TOI-3714 to prevent

significant orbital decay. Future releases from Gaia will provide data to constrain the orbit of the white dwarf companion.

5.4. Comparison to the M dwarf planet population

With the discovery of TOI-3714.01 and TOI-3629.01, there are 8 M dwarf systems hosting transiting hot Jupiters ($P < 10$ days and $R_p > 8R_{\oplus}$). Figure 12 compares the properties of these two systems with the planetary mass-radius, stellar $T_e - \log g_*$, and the insolation flux of other M dwarf systems. All M dwarfs with transiting hot Jupiter-sized gas giants, including TOI-3714.01 and TOI-3629.01, are early M dwarfs (M0-M3). This may simply be an observational bias or a result of a small population size, but in the framework of core accretion, factors such as protoplanetary disk mass may impact the formation of gas giants (e.g., Mordasini et al. 2012; Hasegawa & Pudritz 2013, 2014; Adibekyan 2019). The protoplanetary disk mass is thought to vary linearly with the mass of the host star (e.g., Andrews et al. 2013), such that the efficiency of gas giant formation is expected to increase when orbiting more massive M dwarfs because the materials that form gas giant cores are more abundant compared to the low-mass protoplanetary disks around later M dwarfs.

In addition to the protoplanetary disk mass, the stellar metallicity has been known to be important for gas giant formation. The planet-metallicity correlation, in which metal-rich stars are more likely to host gas giant planets, has been extensively observed in Sun-like stars (e.g., Fischer & Valenti 2005; Johnson et al. 2010; Guo et al. 2017; Osborn & Bayliss 2020). RV studies (e.g., Neves et al. 2013; Maldonado et al. 2020) have suggested the planet-metallicity correlation exists for M dwarfs but there is no statistical study for transiting M dwarfs because of the small population size. Figure 13 compares the metallicity and planetary radii

of these two systems with transiting exoplanets from the NASA Exoplanet Archive. All M dwarfs hosting a transiting Jupiter-sized planet ($R \geq 8 R_{\oplus}$), including TOI-3714 and TOI-3629, have metallicities of $[Fe/H] > 0$.

However, the population of gas giants transiting M dwarfs is small and this may be an observational bias. The metallicities on the NASA Exoplanet Archive are also not homogeneously derived. Metallicities derived using different techniques or instruments may exhibit offsets (e.g., Guo et al. 2017; Petigura et al. 2018). A magnitude limited search from a non-targeted transit survey, such as TESS, to identify a population of hot Jupiters orbiting M dwarfs is required to statistically evaluate if the planet-metallicity and stellar mass correlations apply to the population of transiting M dwarf gas giants. TESS is an ideal mission for this study, as it has been shown to be complete for hot Jupiters transiting earlier Sun-like stars (Zhou et al. 2019) and it should detect almost all transiting hot Jupiter - M dwarf systems given the large transit depth. This population of hot Jupiters could then be extensively studied to provide statistical constraints on the existence and strength of correlations of gas giant planets with metallicity or stellar mass.

TOI-3714 and TOI-3629, like the six existing M dwarf systems with transiting hot Jupiters, also lack additional transiting planets on nearby orbits. Only four hot Jupiters are known to exist in compact multiplanet systems: WASP-47 b (Becker et al. 2015), Kepler-730 b (Zhu et al. 2018; Cañas et al. 2019), TOI-1130 c (Huang et al. 2020c), and WASP-148 b (Wang et al. 2021a). This apparent low multiplicity rate for hot Jupiters orbiting Sun-like stars has been detected in the analysis of multiple statistical samples from ground and space-based transiting hot Jupiters (e.g., Steffen et al. 2012; Huang et al. 2016; Maciejewski 2020; Hord et al. 2021; Wang et al. 2021b; Zhu & Dong 2021). The ap-

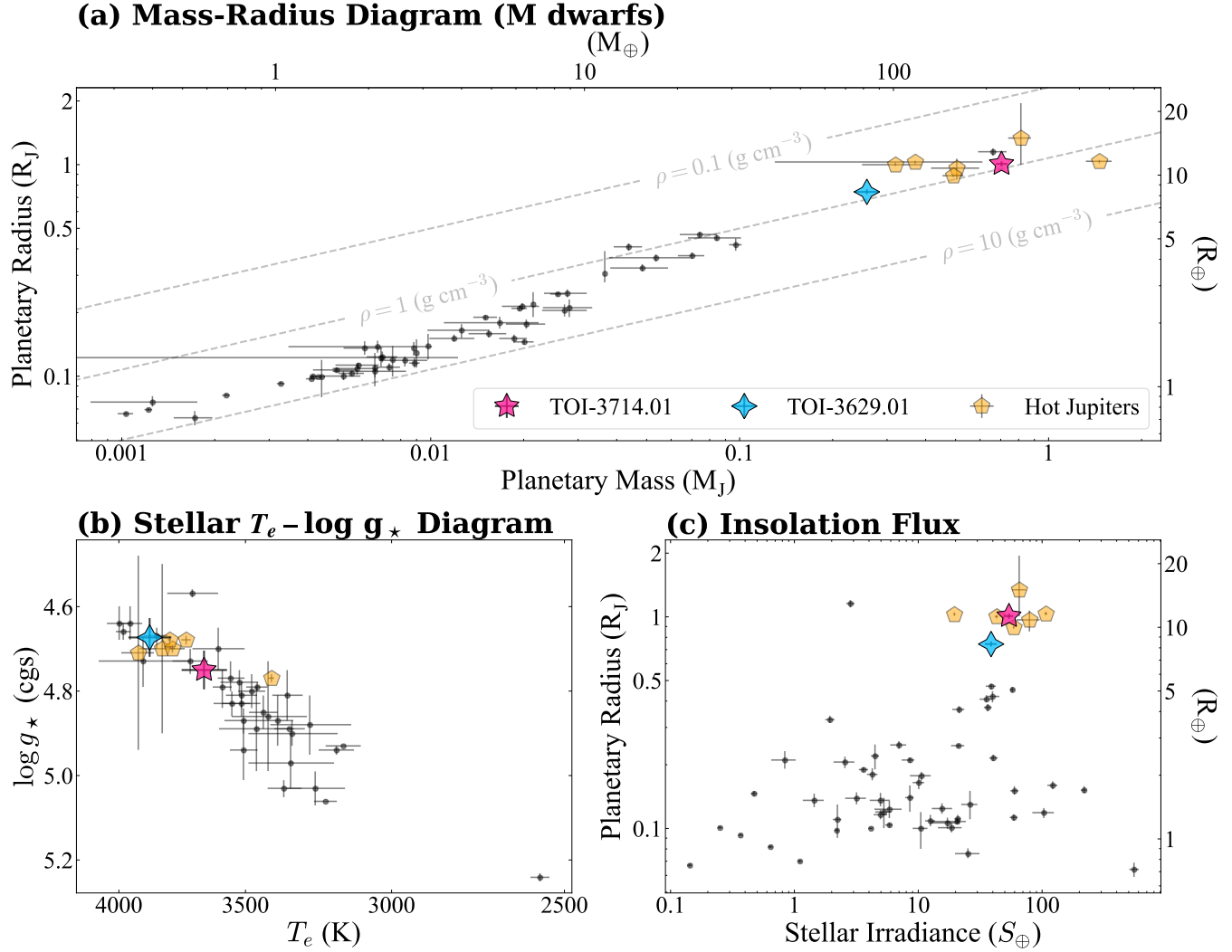


Figure 12. The physical parameters of the TOI-3714 and TOI-3629 systems. (a) places TOI-3714.01 (star) and TOI-3629.01 (diamond star) on the mass-radius diagram for transiting M dwarf exoplanets with mass measurements. The six previously known hot Jupiters ($P < 10$ days and $R_P \geq 8 R_{\oplus}$) transiting M dwarfs are marked as pentagons. Contours of fixed bulk density are plotted for reference. (b) highlights the position of TOI-3714 and TOI-3629 on an effective temperature – surface gravity diagram. (c) presents the insolation flux for M dwarf exoplanets. The data were compiled from the [NASA Exoplanet Archive](#) (Akeson et al. 2013) on 2021 December 27.

parent lack of close-period companions to hot Jupiters may be imprints of high-eccentricity migration (e.g., Mustill et al. 2015; Dawson & Johnson 2018), as this mechanism would destabilize shorter period planets. TOI-3714 and TOI-3629 were observed in long-cadence mode for one sector of TESS data and future photometry observations with TESS could establish whether there are any low S/N transiting planets on close-period orbits.

5.5. Comparison to planetary models

The equilibrium temperatures of TOI-3714.01 and TOI-3629.01 are < 1000 K and it is unlikely these planets exhibit radius inflation due to stellar flux-driven mechanisms. Studies of the population of Kepler hot Jupiters (e.g., Demory & Seager 2011) determined that gas giants receiving an incident flux $\lesssim 2 \times 10^8 \text{ erg s}^{-1} \text{ cm}^{-2}$ have radii that are independent of the stellar incident flux. More recent analyses on transiting

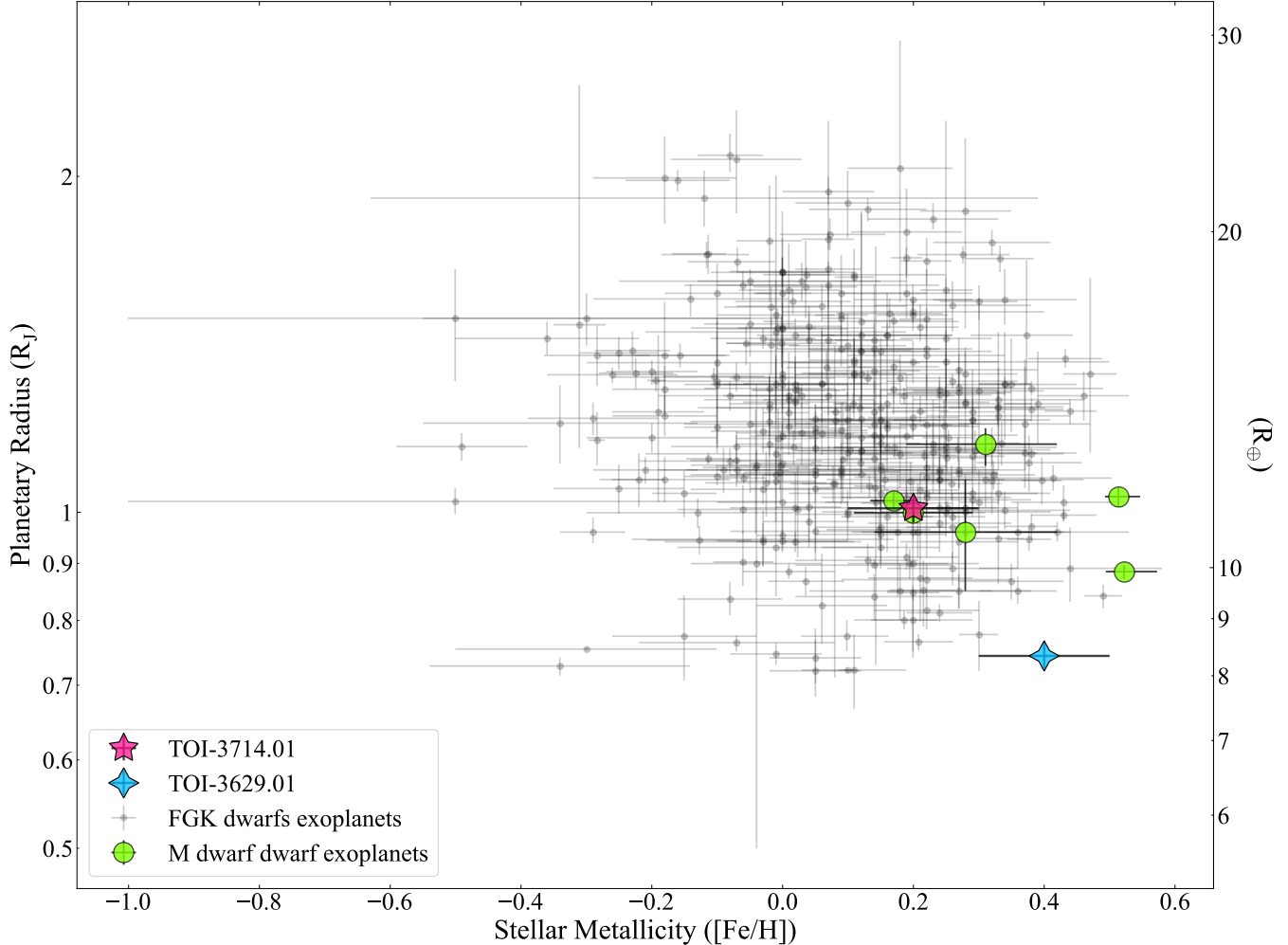


Figure 13. The position of TOI-3714 and TOI-3629 on a metallicity-mass diagram for transiting Jupiter-sized ($R \geq 8 R_{\oplus}$) exoplanets. All known hot Jupiters transiting M dwarfs have $[Fe/H] > 0$. The data were compiled from the [NASA Exoplanet Archive](#) on 2021 December 27.

hot Jupiters (e.g., Thorngren & Fortney 2018; Thorngren et al. 2021) have confirmed that inflated radii are evident in the population of hot Jupiters with $T_{eq} > 1000$ K serving as a threshold for the onset of Ohmic heating and planetary inflation (e.g., Batygin & Stevenson 2010; Miller & Fortney 2011; Batygin et al. 2011).

Both the hot Jupiters TOI-3714.01 and TOI-3629.01 have $T_{eq} < 1000$ K and do not show anomalously large radii when compared to models for gas giants from Baraffe et al. (2008) and Fortney et al. (2007). Although these models are generated for the population of hot Jupiters transiting Sun-like stars, both TOI-3714 and TOI-3629 are in agreement with the

non-irradiated models for gas giant interiors. We compared the observed radii of TOI-3714.01 and TOI-3629.01 to the radius predicted from 1 Gyr models for a solar metallicity atmosphere. The mass and radius of TOI-3714.01 are in agreement with the models from Baraffe et al. (2008) containing a small fraction of heavy metals ($\sim 2\%$) and with the Fortney et al. (2007) models for a core mass of 2 – 4% of the planetary mass. The mass and radius of TOI-3629 are consistent with models from Fortney et al. (2007) having a core mass $\sim 30\%$ of the planetary mass or the Baraffe et al. (2008) models for with a heavy metal fraction of $\sim 20 – 40\%$. These heavy metal fractions are consistent with

what is seen in Jupiter (< 10% core mass; Wahl et al. 2017) and Saturn ($\sim 20\%$; Mankovich & Fuller 2021) in the Solar System.

5.6. Future Characterization

5.6.1. Stellar Obliquity

The projected stellar obliquity (λ) is the apparent angle between the stellar rotation axis and the normal to the planet of the orbit. It can shed light on the dynamical and formation history of planets (e.g., Albrecht et al. 2012; Winn & Fabrycky 2015; Triaud 2018; Albrecht et al. 2021). Measurements of λ for hot Jupiters orbiting Sun-like stars (e.g., Albrecht et al. 2012; Dawson 2014) have revealed an obliquity distribution that is consistent with tidal realignment, indicating that their origin channels most likely involve dynamical interactions, such as planet-planet scattering. To date, there is no measurement of λ for any M dwarf hosting a hot Jupiter. The measurement of λ for either system via the Rossiter-McLaughlin (RM) effect (Triaud 2018) could limit the physical processes involved during formation because some mechanisms, such as disk migration, prohibit highly misaligned orbits (see Dawson & Johnson 2018).

The amplitude of the RM effect can be estimated as $\Delta V = 2/3(R_p/R_*)^2 v \sin i_* \sqrt{1 - b^2}$ (Equation 1, Triaud 2018). For TOI-3714, we estimate an equatorial ($\sin i = 1$) rotational velocity of $v_{eq} = 1.08 \pm 0.06 \text{ km s}^{-1}$ using the derived rotation period and stellar radius. Additional photometric observations of TOI-3629 are required to determine the rotation period, however, if we assume $P_{rot} = 30$ days then the equatorial rotational velocity would be $v_{eq} = 1 \text{ km s}^{-1}$. The estimated RM effect amplitudes would be $\sim 30 \text{ m s}^{-1}$ and $\sim 10 \text{ m s}^{-1}$ for TOI-3714 and TOI-3629, respectively. The precision to detect these amplitudes can be achieved using current high-resolution spectrographs with extended red wavelength coverage because both

of these targets are early M dwarfs with a peak in the SED at around $\sim 0.8 - 0.9$ microns.

5.6.2. Transmission Spectroscopy

TOI-3714 and TOI-3629 are the two brightest M dwarfs ($J < 12$) with a transiting hot Jupiter and are potential targets to probe the atmosphere of temperate ($T_{eq} < 800 \text{ K}$) M dwarf - hot Jupiter systems. Sing et al. (2016) obtained transmission spectra of hot Jupiters transiting Sun-like stars and noticed the observed sample contained both cloudy and clear planets, suggesting that hot Jupiters did not exhibit a strong relationship to cloud formation. No extensive studies have been performed on M dwarf hot Jupiters.

TOI-3714 and TOI-3629 provide an opportunity to examine the prevalence of clouds and photochemical hazes for M dwarf exoplanets. Under certain combinations of temperature and surface gravity, clouds or hazes may form in the visible region of a hot Jupiter atmosphere either through condensation chemistry or photochemical processes (e.g., Sudarsky et al. 2003; Helling et al. 2008; Marley et al. 2013) and the presence of clouds or hazes may weaken or mask spectral features (Sing et al. 2016; Sing 2018). Photochemical processes are more efficient in cooler exoplanets (e.g., Moses et al. 2011) and high incident stellar UV irradiation is thought to enhance the photochemical production of hydrocarbon aerosol (e.g., Liang et al. 2004; Line et al. 2010). Transmission spectra of TOI-3714.01 and TOI-3629.01 with the James Webb Space Telescope (JWST; Gardner et al. 2006) would probe atmospheric chemistry of gas giants orbiting M dwarfs and the effects of higher UV radiation environment of early M dwarfs on atmospheric chemistry (e.g., Pineda et al. 2021).

6. SUMMARY

We report the discovery of two gas giants orbiting M dwarfs. TOI-3714.01 is a hot Jupiter ($M_p = 0.70 \pm 0.03 M_J$ and $R_p = 1.01 \pm 0.03 R_J$)

on a $P = 2.154849 \pm 0.000001$ day orbit. TOI-3629.01 is a hot Jupiter ($M_p = 0.26 \pm 0.02M_J$ and $R_p = 0.74 \pm 0.02R_J$) on a $P = 3.936551^{+0.000005}_{-0.000006}$ day orbit. Only TOI-3714 has a detectable rotation period of 23.4 ± 0.9 days and most probably has an age between $0.7 - 5.1$ Gyrs. All hot Jupiters known to transit M dwarfs, including TOI-3714 and TOI-3629, orbit metal-rich early M dwarfs (M0-M3). A larger population size and homogeneously derived metallicities are required to confirm if the correlations with metallicity and stellar mass observed for hot Jupiters orbiting Sun-like stars are also observed in the population of M dwarf gas giants. Constraints from Gaia EDR3 and RVs reject the presence of massive short-period companions to both gas giants, but TOI-3714 has a resolved white dwarf companion at a projected separation of ~ 300 au. The progenitor may have been close enough to impact the orbit of a nascent TOI-3714.01 as it evolved into a white dwarf, but constraints on the astrometric orbit from future Gaia observations are required to examine this. TOI-3714 and TOI-3629 are the brightest M dwarfs hosting hot Jupiters ($J < 12$) and are amenable to observations during transit to (i) further our understanding of their dynamical history with a measurement of the projected obliquity and (ii) explore the atmospheric chemistry of hot gas giants orbiting cool stars.

Acknowledgments. CIC acknowledges support by NASA Headquarters under the NASA Earth and Space Science Fellowship Program through grant 80NSSC18K1114, the Alfred P. Sloan Foundation's Minority Ph.D. Program through grant G-2016-20166039, and the Pennsylvania State University's Bunton-Waller program. The Center for Exoplanets and Habitable Worlds is supported by the Pennsylvania State University and the Eberly College of Science. The computations for this research were performed on the Pennsylvania State University's Institute

for Computational and Data Sciences' Roar supercomputer, including the CyberLAMP cluster supported by NSF grant MRI-1626251. This content is solely the responsibility of the authors and does not necessarily represent the views of the Institute for Computational and Data Sciences. TNS acknowledges support from the Wyoming Research Scholars Program.

We acknowledge support from NSF grants AST 1006676, AST 1126413, AST 1310875, AST 1310885, AST 2009889 and the NASA Astrobiology Institute (NNA09DA76A) in our pursuit of precision RVs in the near-infrared. We acknowledge support from the Heising-Simons Foundation via grant 2017-0494. We acknowledge support from NSF grants AST 1907622, AST 1909506, AST 1909682, AST 1910954 and the Research Corporation in connection with precision diffuser-assisted photometry.

This work is Contribution 0046 from the Center for Planetary Systems Habitability at the University of Texas at Austin. These results are based on observations obtained with HPF on the HET. The HET is a joint project of the University of Texas at Austin, the Pennsylvania State University, Ludwig-Maximilians-Universität München, and Georg-August Universität Gottingen. The HET is named in honor of its principal benefactors, William P. Hobby and Robert E. Eberly. The HET collaboration acknowledges the support and resources from the Texas Advanced Computing Center. We are grateful to the HET Resident Astronomers and Telescope Operators for their valuable assistance in gathering our HPF data. We would like to acknowledge that the HET is built on Indigenous land. Moreover, we would like to acknowledge and pay our respects to the Carrizo & Comecrudo, Coahuiltecan, Caddo, Tonkawa, Comanche, Lipan Apache, Alabama-Coushatta, Kickapoo, Tigua Pueblo, and all the American Indian and Indigenous Peoples and communities

who have been or have become a part of these lands and territories in Texas, here on Turtle Island.

Some of the data presented were obtained by the NEID spectrograph built by the Pennsylvania State University and operated at the WIYN Observatory by NOIRLab, under the NN-EXPLORE partnership of NASA and the NSF. These results are also based on observations obtained with NEID on the WIYN 3.5m telescope at KPNO, NSF's NOIRLab under proposals 2021B-0035 (PI: S. Kanodia), 2021B-0435 (PI: S. Kanodia), and 2021B-0438 (PI: C. Cañas), managed by the Association of Universities for Research in Astronomy (AURA) under a cooperative agreement with the NSF. This work was performed for the Jet Propulsion Laboratory, California Institute of Technology, sponsored by the United States Government under the Prime Contract 80NM0018D0004 between Caltech and NASA. WIYN is a joint facility of the University of Wisconsin-Madison, Indiana University, NSF's NOIRLab, the Pennsylvania State University, Purdue University, University of California-Irvine, and the University of Missouri. The authors are honored to be permitted to conduct astronomical research on Iolkam Du'ag (Kitt Peak), a mountain with particular significance to the Tohono O'odham. Data presented herein were obtained at the WIYN Observatory from telescope time allocated to NN-EXPLORE through the scientific partnership of NASA, the NSF, and NOIRLab.

Some of results are based on observations obtained with the Apache Point Observatory 3.5m telescope, which is owned and operated by the Astrophysical Research Consortium. We wish to thank the APO 3.5m telescope operators in their assistance in obtaining these data.

Some of the observations in this paper made use of the NN-EXPLORE Exoplanet and Stellar Speckle Imager (NESSI). NESSI was funded by

the NASA Exoplanet Exploration Program and the NASA Ames Research Center. NESSI was built at the Ames Research Center by Steve B. Howell, Nic Scott, Elliott P. Horch, and Emmett Quigley.

Some of the data presented in this paper were obtained from MAST at STScI. Support for MAST for non-HST data is provided by the NASA Office of Space Science via grant NNX09AF08G and by other grants and contracts. This work includes data collected by the TESS mission, which are publicly available from MAST. Funding for the TESS mission is provided by the NASA Science Mission directorate. This research made use of the (i) NASA Exoplanet Archive, which is operated by Caltech, under contract with NASA under the Exoplanet Exploration Program, (ii) SIMBAD database, operated at CDS, Strasbourg, France, (iii) NASA's Astrophysics Data System Bibliographic Services, (iv) NASA/IPAC Infrared Science Archive, which is funded by NASA and operated by the California Institute of Technology, and (v) data from 2MASS, a joint project of the University of Massachusetts and IPAC at Caltech, funded by NASA and the NSF.

This work has made use of data from the European Space Agency (ESA) mission Gaia (<https://www.cosmos.esa.int/gaia>), processed by the Gaia Data Processing and Analysis Consortium (DPAC, <https://www.cosmos.esa.int/web/gaia/dpac/consortium>). Funding for the DPAC has been provided by national institutions, in particular the institutions participating in the Gaia Multilateral Agreement.

Some of the observations in this paper made use of the Guoshoujing Telescope (LAMOST), a National Major Scientific Project built by the Chinese Academy of Sciences. Funding for the project has been provided by the National Development and Reform Commission. LAMOST is operated and managed by the National As-

trononical Observatories, Chinese Academy of Sciences.

Some of the observations in this paper were obtained with the Samuel Oschin Telescope 48-inch and the 60-inch Telescope at the Palomar Observatory as part of the ZTF project. ZTF is supported by the NSF under Grant No. AST-2034437 and a collaboration including Caltech, IPAC, the Weizmann Institute for Science, the Oskar Klein Center at Stockholm University, the University of Maryland, Deutsches Elektronen-Synchrotron and Humboldt University, the TANGO Consortium of Taiwan, the University of Wisconsin at Milwaukee, Trinity College Dublin, Lawrence Livermore National Laboratories, and IN2P3, France. Operations are conducted by COO, IPAC, and UW.

Facilities: ARC (ARCTIC), Exoplanet Archive, Gaia, HET (HPF), IRSA, KPNO:2.1m

(Robo-AO), LAMOST, MAST, PO:1.2m (ZTF), PO:1.5m (ZTF), SO:Kuiper, TESS, WIYN (NEID, NESSI)

Software: `astroquery` (Ginsburg et al. 2019), `astropy` (Astropy Collaboration et al. 2018), `barycorrpy` (Kanodia & Wright 2018), `dynesty` (Speagle 2020), `EXOFASTv2` (Eastman et al. 2019), `GLS` (Zechmeister & Kürster 2009), `HPF-SpecMatch` (S. Jones et al. 2022), `juliet` (Espinoza et al. 2019), `lightkurve` (Lightkurve Collaboration et al. 2018), `matplotlib` (Hunter 2007), `numpy` (van der Walt et al. 2011), `pandas` (McKinney 2010), `scipy` (Virtanen et al. 2020), `telfit` (Gullikson et al. 2014), `thejoker` (Price-Whelan et al. 2017), `WD_models` (Cheng et al. 2019)

REFERENCES

- Adibekyan, V. 2019, Geosciences, 9, 105, doi: [10.3390/geosciences9030105](https://doi.org/10.3390/geosciences9030105)
- Akeson, R. L., Chen, X., Ciardi, D., et al. 2013, PASP, 125, 989, doi: [10.1086/672273](https://doi.org/10.1086/672273)
- Albrecht, S., Winn, J. N., Johnson, J. A., et al. 2012, ApJ, 757, 18, doi: [10.1088/0004-637X/757/1/18](https://doi.org/10.1088/0004-637X/757/1/18)
- Albrecht, S. H., Marcussen, M. L., Winn, J. N., Dawson, R. I., & Knudstrup, E. 2021, arXiv e-prints, arXiv:2105.09327. <https://arxiv.org/abs/2105.09327>
- Anderson, K. R., Storch, N. I., & Lai, D. 2016, MNRAS, 456, 3671, doi: [10.1093/mnras/stv2906](https://doi.org/10.1093/mnras/stv2906)
- Andrews, S. M., Rosenfeld, K. A., Kraus, A. L., & Wilner, D. J. 2013, ApJ, 771, 129, doi: [10.1088/0004-637X/771/2/129](https://doi.org/10.1088/0004-637X/771/2/129)
- Anglada-Escudé, G., & Butler, R. P. 2012, ApJS, 200, 15, doi: [10.1088/0067-0049/200/2/15](https://doi.org/10.1088/0067-0049/200/2/15)
- Angus, R., Morton, T., Aigrain, S., Foreman-Mackey, D., & Rajpaul, V. 2018, MNRAS, 474, 2094, doi: [10.1093/mnras/stx2109](https://doi.org/10.1093/mnras/stx2109)
- Astropy Collaboration, Price-Whelan, A. M., Sipőcz, B. M., et al. 2018, AJ, 156, 123, doi: [10.3847/1538-3881/aabc4f](https://doi.org/10.3847/1538-3881/aabc4f)
- Bailer-Jones, C. A. L., Rybizki, J., Fouesneau, M., Demleitner, M., & Andrae, R. 2021, AJ, 161, 147, doi: [10.3847/1538-3881/abd806](https://doi.org/10.3847/1538-3881/abd806)
- Bakos, G. Á., Bayliss, D., Bento, J., et al. 2020, AJ, 159, 267, doi: [10.3847/1538-3881/ab8ad1](https://doi.org/10.3847/1538-3881/ab8ad1)
- Baraffe, I., Chabrier, G., & Barman, T. 2008, A&A, 482, 315, doi: [10.1051/0004-6361:20079321](https://doi.org/10.1051/0004-6361:20079321)
- Baranec, C., Riddle, R., Law, N. M., et al. 2013, Journal of Vibration Engineering, 72, 50021, doi: [10.3791/50021](https://doi.org/10.3791/50021)
- . 2014, ApJL, 790, L8, doi: [10.1088/2041-8205/790/1/L8](https://doi.org/10.1088/2041-8205/790/1/L8)
- Batygin, K., Bodenheimer, P. H., & Laughlin, G. P. 2016, ApJ, 829, 114, doi: [10.3847/0004-637X/829/2/114](https://doi.org/10.3847/0004-637X/829/2/114)
- Batygin, K., & Stevenson, D. J. 2010, ApJL, 714, L238, doi: [10.1088/2041-8205/714/2/L238](https://doi.org/10.1088/2041-8205/714/2/L238)
- Batygin, K., Stevenson, D. J., & Bodenheimer, P. H. 2011, ApJ, 738, 1, doi: [10.1088/0004-637X/738/1/1](https://doi.org/10.1088/0004-637X/738/1/1)
- Bayliss, D., Gillen, E., Eigmüller, P., et al. 2018, MNRAS, 475, 4467, doi: [10.1093/mnras/stx2778](https://doi.org/10.1093/mnras/stx2778)

- Becker, J. C., Vanderburg, A., Adams, F. C., Rappaport, S. A., & Schwengeler, H. M. 2015, ApJL, 812, L18, doi: [10.1088/2041-8205/812/2/L18](https://doi.org/10.1088/2041-8205/812/2/L18)
- Bédard, A., Bergeron, P., Brassard, P., & Fontaine, G. 2020, ApJ, 901, 93, doi: [10.3847/1538-4357/abafbe](https://doi.org/10.3847/1538-4357/abafbe)
- Belokurov, V., Penoyre, Z., Oh, S., et al. 2020, MNRAS, 496, 1922, doi: [10.1093/mnras/staa1522](https://doi.org/10.1093/mnras/staa1522)
- Bensby, T., Feltzing, S., & Lundström, I. 2003, A&A, 410, 527, doi: [10.1051/0004-6361:20031213](https://doi.org/10.1051/0004-6361:20031213)
- Bessell, M. S. 1990, PASP, 102, 1181, doi: [10.1086/132749](https://doi.org/10.1086/132749)
- Boley, A. C., Granados Contreras, A. P., & Gladman, B. 2016, ApJL, 817, L17, doi: [10.3847/2041-8205/817/2/L17](https://doi.org/10.3847/2041-8205/817/2/L17)
- Bonfils, X., Delfosse, X., Udry, S., et al. 2013, A&A, 549, A109, doi: [10.1051/0004-6361/201014704](https://doi.org/10.1051/0004-6361/201014704)
- Bovy, J. 2015, ApJS, 216, 29, doi: [10.1088/0067-0049/216/2/29](https://doi.org/10.1088/0067-0049/216/2/29)
- Brasseur, C. E., Phillip, C., Fleming, S. W., Mullally, S. E., & White, R. L. 2019, Astrocute: Tools for creating cutouts of TESS images. <http://ascl.net/1905.007>
- Butler, R. P., Wright, J. T., Marcy, G. W., et al. 2006, ApJ, 646, 505, doi: [10.1086/504701](https://doi.org/10.1086/504701)
- Cañas, C. I., Wang, S., Mahadevan, S., et al. 2019, ApJ, 870, L17, doi: [10.3847/2041-8213/aafale](https://doi.org/10.3847/2041-8213/aafale)
- Cañas, C. I., Stefánsson, G., Kanodia, S., et al. 2020, AJ, 160, 147, doi: [10.3847/1538-3881/abac67](https://doi.org/10.3847/1538-3881/abac67)
- Canto Martins, B. L., Gomes, R. L., Messias, Y. S., et al. 2020, ApJS, 250, 20, doi: [10.3847/1538-4365/aba73f](https://doi.org/10.3847/1538-4365/aba73f)
- Cheng, S., Cummings, J. D., & Ménard, B. 2019, ApJ, 886, 100, doi: [10.3847/1538-4357/ab4989](https://doi.org/10.3847/1538-4357/ab4989)
- Choi, J., Dotter, A., Conroy, C., et al. 2016, ApJ, 823, 102, doi: [10.3847/0004-637X/823/2/102](https://doi.org/10.3847/0004-637X/823/2/102)
- Collins, K. A., Kielkopf, J. F., Stassun, K. G., & Hessman, F. V. 2017, AJ, 153, 77, doi: [10.3847/1538-3881/153/2/77](https://doi.org/10.3847/1538-3881/153/2/77)
- Cui, X.-Q., Zhao, Y.-H., Chu, Y.-Q., et al. 2012, Research in Astronomy and Astrophysics, 12, 1197, doi: [10.1088/1674-4527/12/9/003](https://doi.org/10.1088/1674-4527/12/9/003)
- Cumming, A., Butler, R. P., Marcy, G. W., et al. 2008, PASP, 120, 531, doi: [10.1086/588487](https://doi.org/10.1086/588487)
- Cummings, J. D., Kalirai, J. S., Tremblay, P. E., Ramirez-Ruiz, E., & Choi, J. 2018, ApJ, 866, 21, doi: [10.3847/1538-4357/aadfd6](https://doi.org/10.3847/1538-4357/aadfd6)
- Cutri, R. M., Skrutskie, M. F., van Dyk, S., et al. 2003, VizieR Online Data Catalog, 2246
- Dawson, R. I. 2014, ApJL, 790, L31, doi: [10.1088/2041-8205/790/2/L31](https://doi.org/10.1088/2041-8205/790/2/L31)
- Dawson, R. I., & Johnson, J. A. 2018, ARA&A, 56, 175, doi: [10.1146/annurev-astro-081817-051853](https://doi.org/10.1146/annurev-astro-081817-051853)
- Demory, B.-O., & Seager, S. 2011, ApJS, 197, 12, doi: [10.1088/0067-0049/197/1/12](https://doi.org/10.1088/0067-0049/197/1/12)
- Desidera, S., & Barbieri, M. 2007, A&A, 462, 345, doi: [10.1051/0004-6361:20066319](https://doi.org/10.1051/0004-6361:20066319)
- Dotter, A. 2016, ApJS, 222, 8, doi: [10.3847/0067-0049/222/1/8](https://doi.org/10.3847/0067-0049/222/1/8)
- Eastman, J. D., Rodriguez, J. E., Agol, E., et al. 2019, arXiv e-prints, arXiv:1907.09480. <https://arxiv.org/abs/1907.09480>
- El-Badry, K., & Rix, H.-W. 2018, MNRAS, 480, 4884, doi: [10.1093/mnras/sty2186](https://doi.org/10.1093/mnras/sty2186)
- El-Badry, K., Rix, H.-W., & Heintz, T. M. 2021, MNRAS, 506, 2269, doi: [10.1093/mnras/stab323](https://doi.org/10.1093/mnras/stab323)
- Endl, M., Cochran, W. D., Kürster, M., et al. 2006, ApJ, 649, 436, doi: [10.1086/506465](https://doi.org/10.1086/506465)
- Engle, S. G., & Guinan, E. F. 2018, Research Notes of the American Astronomical Society, 2, 34, doi: [10.3847/2515-5172/aab1f8](https://doi.org/10.3847/2515-5172/aab1f8)
- Espinoza, N., Kossakowski, D., & Brahm, R. 2019, MNRAS, 490, 2262, doi: [10.1093/mnras/stz2688](https://doi.org/10.1093/mnras/stz2688)
- Fabrycky, D., & Tremaine, S. 2007, ApJ, 669, 1298, doi: [10.1086/521702](https://doi.org/10.1086/521702)
- Farihi, J., Bond, H. E., Dufour, P., et al. 2013, MNRAS, 430, 652, doi: [10.1093/mnras/sts677](https://doi.org/10.1093/mnras/sts677)
- Farihi, J., Burleigh, M. R., Holberg, J. B., Casewell, S. L., & Barstow, M. A. 2011, MNRAS, 417, 1735, doi: [10.1111/j.1365-2966.2011.19354.x](https://doi.org/10.1111/j.1365-2966.2011.19354.x)
- Feinstein, A. D., Montet, B. T., Foreman-Mackey, D., et al. 2019, PASP, 131, 094502, doi: [10.1088/1538-3873/ab291c](https://doi.org/10.1088/1538-3873/ab291c)
- Fischer, D. A., & Valenti, J. 2005, ApJ, 622, 1102, doi: [10.1086/428383](https://doi.org/10.1086/428383)
- Fitzpatrick, E. L. 1999, PASP, 111, 63, doi: [10.1086/316293](https://doi.org/10.1086/316293)
- Fontanive, C., & Bardalez Gagliuffi, D. 2021, Frontiers in Astronomy and Space Sciences, 8, 16, doi: [10.3389/fspas.2021.625250](https://doi.org/10.3389/fspas.2021.625250)
- Ford, E. B., & Rasio, F. A. 2008, ApJ, 686, 621, doi: [10.1086/590926](https://doi.org/10.1086/590926)

- Foreman-Mackey, D., Agol, E., Ambikasaran, S., & Angus, R. 2017, AJ, 154, 220, doi: [10.3847/1538-3881/aa9332](https://doi.org/10.3847/1538-3881/aa9332)
- Fortney, J. J., Marley, M. S., & Barnes, J. W. 2007, ApJ, 659, 1661, doi: [10.1086/512120](https://doi.org/10.1086/512120)
- Fulton, B. J., Petigura, E. A., Blunt, S., & Sinukoff, E. 2018, PASP, 130, 044504, doi: [10.1088/1538-3873/aaaaaa8](https://doi.org/10.1088/1538-3873/aaaaaa8)
- Gagné, J., Mamajek, E. E., Malo, L., et al. 2018, ApJ, 856, 23, doi: [10.3847/1538-4357/aaae09](https://doi.org/10.3847/1538-4357/aaae09)
- Gaia Collaboration, Brown, A. G. A., Vallenari, A., et al. 2021, A&A, 649, A1, doi: [10.1051/0004-6361/202039657](https://doi.org/10.1051/0004-6361/202039657)
- Gandhi, P., Buckley, D. A. H., Charles, P., et al. 2020, arXiv e-prints, arXiv:2009.07277. <https://arxiv.org/abs/2009.07277>
- Gandolfi, D., Barragán, O., Livingston, J. H., et al. 2018, A&A, 619, L10, doi: [10.1051/0004-6361/201834289](https://doi.org/10.1051/0004-6361/201834289)
- Gardner, J. P., Mather, J. C., Clampin, M., et al. 2006, SSRv, 123, 485, doi: [10.1007/s11214-006-8315-7](https://doi.org/10.1007/s11214-006-8315-7)
- Gentile Fusillo, N. P., Tremblay, P. E., Cukanovaite, E., et al. 2021, MNRAS, 508, 3877, doi: [10.1093/mnras/stab2672](https://doi.org/10.1093/mnras/stab2672)
- Ginsburg, A., Sipőcz, B. M., Brasseur, C. E., et al. 2019, AJ, 157, 98, doi: [10.3847/1538-3881/aafc33](https://doi.org/10.3847/1538-3881/aafc33)
- Green, G. M., Schlafly, E., Zucker, C., Speagle, J. S., & Finkbeiner, D. 2019, ApJ, 887, 93, doi: [10.3847/1538-4357/ab5362](https://doi.org/10.3847/1538-4357/ab5362)
- Gullikson, K., Dodson-Robinson, S., & Kraus, A. 2014, AJ, 148, 53, doi: [10.1088/0004-6256/148/3/53](https://doi.org/10.1088/0004-6256/148/3/53)
- Guo, X., Johnson, J. A., Mann, A. W., et al. 2017, ApJ, 838, 25, doi: [10.3847/1538-4357/aa6004](https://doi.org/10.3847/1538-4357/aa6004)
- Halverson, S., Terrien, R., Mahadevan, S., et al. 2016, Society of Photo-Optical Instrumentation Engineers (SPIE) Conference Series, Vol. 9908, A comprehensive radial velocity error budget for next generation Doppler spectrometers, 99086P, doi: [10.1117/12.2232761](https://doi.org/10.1117/12.2232761)
- Hartman, J. D., Bayliss, D., Brahm, R., et al. 2015, AJ, 149, 166, doi: [10.1088/0004-6256/149/5/166](https://doi.org/10.1088/0004-6256/149/5/166)
- Hasegawa, Y., & Pudritz, R. E. 2013, ApJ, 778, 78, doi: [10.1088/0004-637X/778/1/78](https://doi.org/10.1088/0004-637X/778/1/78)
- . 2014, ApJ, 794, 25, doi: [10.1088/0004-637X/794/1/25](https://doi.org/10.1088/0004-637X/794/1/25)
- Helling, C., Woitke, P., & Thi, W. F. 2008, A&A, 485, 547, doi: [10.1051/0004-6361:20078220](https://doi.org/10.1051/0004-6361:20078220)
- Henden, A. A., Levine, S., Terrell, D., et al. 2018, in American Astronomical Society Meeting Abstracts, Vol. 232, American Astronomical Society Meeting Abstracts #232, 223.06
- Henry, T. J., Jao, W.-C., Winters, J. G., et al. 2018, AJ, 155, 265, doi: [10.3847/1538-3881/aac262](https://doi.org/10.3847/1538-3881/aac262)
- Hord, B. J., Colón, K. D., Kostov, V., et al. 2021, AJ, 162, 263, doi: [10.3847/1538-3881/ac2602](https://doi.org/10.3847/1538-3881/ac2602)
- Howard, A. W., Marcy, G. W., Bryson, S. T., et al. 2012, ApJS, 201, 15, doi: [10.1088/0067-0049/201/2/15](https://doi.org/10.1088/0067-0049/201/2/15)
- Howell, S. B., Everett, M. E., Sherry, W., Horch, E., & Ciardi, D. R. 2011, AJ, 142, 19, doi: [10.1088/0004-6256/142/1/19](https://doi.org/10.1088/0004-6256/142/1/19)
- Huang, C., Wu, Y., & Triaud, A. H. M. J. 2016, ApJ, 825, 98, doi: [10.3847/0004-637X/825/2/98](https://doi.org/10.3847/0004-637X/825/2/98)
- Huang, C. X., Vanderburg, A., Pál, A., et al. 2020a, Research Notes of the American Astronomical Society, 4, 204, doi: [10.3847/2515-5172/abca2e](https://doi.org/10.3847/2515-5172/abca2e)
- . 2020b, Research Notes of the American Astronomical Society, 4, 206, doi: [10.3847/2515-5172/abca2d](https://doi.org/10.3847/2515-5172/abca2d)
- Huang, C. X., Quinn, S. N., Vanderburg, A., et al. 2020c, ApJL, 892, L7, doi: [10.3847/2041-8213/ab7302](https://doi.org/10.3847/2041-8213/ab7302)
- Hubickyj, O., Bodenheimer, P., & Lissauer, J. J. 2005, Icarus, 179, 415, doi: [10.1016/j.icarus.2005.06.021](https://doi.org/10.1016/j.icarus.2005.06.021)
- Huehnerhoff, J., Ketzeback, W., Bradley, A., et al. 2016, in Society of Photo-Optical Instrumentation Engineers (SPIE) Conference Series, Vol. 9908, Ground-based and Airborne Instrumentation for Astronomy VI, ed. C. J. Evans, L. Simard, & H. Takami, 99085H, doi: [10.1117/12.2234214](https://doi.org/10.1117/12.2234214)
- Hunter, J. D. 2007, Computing In Science & Engineering, 9, 90, doi: [10.1109/MCSE.2007.55](https://doi.org/10.1109/MCSE.2007.55)
- Ida, S., & Lin, D. N. C. 2004, ApJ, 616, 567, doi: [10.1086/424830](https://doi.org/10.1086/424830)
- . 2005, ApJ, 626, 1045, doi: [10.1086/429953](https://doi.org/10.1086/429953)
- Ivanova, N., Justham, S., Chen, X., et al. 2013, A&A Rv, 21, 59, doi: [10.1007/s00159-013-0059-2](https://doi.org/10.1007/s00159-013-0059-2)
- Jenkins, J. M., Caldwell, D. A., Chandrasekaran, H., et al. 2010, ApJL, 713, L87, doi: [10.1088/2041-8205/713/2/L87](https://doi.org/10.1088/2041-8205/713/2/L87)

- Jensen-Clem, R., Duev, D. A., Riddle, R., et al. 2018, AJ, 155, 32, doi: [10.3847/1538-3881/aa9be6](https://doi.org/10.3847/1538-3881/aa9be6)
- Johnson, D. R. H., & Soderblom, D. R. 1987, AJ, 93, 864, doi: [10.1086/114370](https://doi.org/10.1086/114370)
- Johnson, J. A., Aller, K. M., Howard, A. W., & Crepp, J. R. 2010, PASP, 122, 905, doi: [10.1086/655775](https://doi.org/10.1086/655775)
- Johnson, J. A., Gazak, J. Z., Apps, K., et al. 2012, AJ, 143, 111, doi: [10.1088/0004-6256/143/5/111](https://doi.org/10.1088/0004-6256/143/5/111)
- Jordán, A., Hartman, J. D., Bayliss, D., et al. 2021, arXiv e-prints, arXiv:2112.01928. <https://arxiv.org/abs/2112.01928>
- Kanodia, S., & Wright, J. 2018, Research Notes of the American Astronomical Society, 2, 4, doi: [10.3847/2515-5172/aaa4b7](https://doi.org/10.3847/2515-5172/aaa4b7)
- Kanodia, S., Mahadevan, S., Ramsey, L. W., et al. 2018, in Society of Photo-Optical Instrumentation Engineers (SPIE) Conference Series, Vol. 10702, Ground-based and Airborne Instrumentation for Astronomy VII, ed. C. J. Evans, L. Simard, & H. Takami, 107026Q, doi: [10.1117/12.2313491](https://doi.org/10.1117/12.2313491)
- Kanodia, S., Cañas, C. I., Stefansson, G., et al. 2020, ApJ, 899, 29, doi: [10.3847/1538-4357/aba0a2](https://doi.org/10.3847/1538-4357/aba0a2)
- Kaplan, K. F., Bender, C. F., Terrien, R. C., et al. 2019, in Astronomical Society of the Pacific Conference Series, Vol. 523, Astronomical Data Analysis Software and Systems XXVII, ed. P. J. Teuben, M. W. Pound, B. A. Thomas, & E. M. Warner, 567
- Kasper, D. H., Ellis, T. G., Yeigh, R. R., et al. 2016, PASP, 128, 105005, doi: [10.1088/1538-3873/128/968/105005](https://doi.org/10.1088/1538-3873/128/968/105005)
- Kennedy, G. M., & Kenyon, S. J. 2008, ApJ, 673, 502, doi: [10.1086/524130](https://doi.org/10.1086/524130)
- Kervella, P., Arenou, F., Mignard, F., & Thévenin, F. 2019, A&A, 623, A72, doi: [10.1051/0004-6361/201834371](https://doi.org/10.1051/0004-6361/201834371)
- Kiefer, F., Hébrard, G., Sahlmann, J., et al. 2019, A&A, 631, A125, doi: [10.1051/0004-6361/201935113](https://doi.org/10.1051/0004-6361/201935113)
- Kipping, D. M. 2013a, MNRAS, 435, 2152, doi: [10.1093/mnras/stt1435](https://doi.org/10.1093/mnras/stt1435)
- . 2013b, MNRAS, 434, L51, doi: [10.1093/mnrasl/slt075](https://doi.org/10.1093/mnrasl/slt075)
- Kiseleva, L. G., Eggleton, P. P., & Mikkola, S. 1998, MNRAS, 300, 292, doi: [10.1046/j.1365-8711.1998.01903.x](https://doi.org/10.1046/j.1365-8711.1998.01903.x)
- Knutson, H. A., Fulton, B. J., Montet, B. T., et al. 2014, ApJ, 785, 126, doi: [10.1088/0004-637X/785/2/126](https://doi.org/10.1088/0004-637X/785/2/126)
- Kovács, G., Zucker, S., & Mazeh, T. 2002, A&A, 391, 369, doi: [10.1051/0004-6361:20020802](https://doi.org/10.1051/0004-6361:20020802)
- Kovács, G., Hodgkin, S., Sipőcz, B., et al. 2013, in European Physical Journal Web of Conferences, Vol. 47, European Physical Journal Web of Conferences, 01002, doi: [10.1051/epjconf/20134701002](https://doi.org/10.1051/epjconf/20134701002)
- Kreidberg, L. 2015, batman: BAsic Transit Model cAlculatioN in Python, Astrophysics Source Code Library. <http://ascl.net/1510.002>
- Kunimoto, M., & Daylan, T. 2021, in Posters from the TESS Science Conference II (TSC2), 62, doi: [10.5281/zenodo.5125527](https://doi.org/10.5281/zenodo.5125527)
- Lamman, C., Baranec, C., Berta-Thompson, Z. K., et al. 2020, AJ, 159, 139, doi: [10.3847/1538-3881/ab6ef1](https://doi.org/10.3847/1538-3881/ab6ef1)
- Laughlin, G., Bodenheimer, P., & Adams, F. C. 2004, ApJL, 612, L73, doi: [10.1086/424384](https://doi.org/10.1086/424384)
- Liang, M.-C., Seager, S., Parkinson, C. D., Lee, A. Y. T., & Yung, Y. L. 2004, ApJL, 605, L61, doi: [10.1086/392509](https://doi.org/10.1086/392509)
- Lightkurve Collaboration, Cardoso, J. V. d. M. a., Hedges, C., et al. 2018, Lightkurve: Kepler and TESS time series analysis in Python. <http://ascl.net/1812.013>
- Lin, D. N. C., Bodenheimer, P., & Richardson, D. C. 1996, Nature, 380, 606, doi: [10.1038/380606a0](https://doi.org/10.1038/380606a0)
- Lindgren, L., Klioner, S. A., Hernández, J., et al. 2021, A&A, 649, A2, doi: [10.1051/0004-6361/202039709](https://doi.org/10.1051/0004-6361/202039709)
- Line, M. R., Liang, M. C., & Yung, Y. L. 2010, ApJ, 717, 496, doi: [10.1088/0004-637X/717/1/496](https://doi.org/10.1088/0004-637X/717/1/496)
- Maciejewski, G. 2020, AcA, 70, 181, doi: [10.32023/0001-5237/70.3.2](https://doi.org/10.32023/0001-5237/70.3.2)
- Mahadevan, S., Ramsey, L., Bender, C., et al. 2012, in Society of Photo-Optical Instrumentation Engineers (SPIE) Conference Series, Vol. 8446, Proc. SPIE, 84461S, doi: [10.1117/12.926102](https://doi.org/10.1117/12.926102)
- Mahadevan, S., Ramsey, L. W., Terrien, R., et al. 2014, in Proc. SPIE, Vol. 9147, Ground-based and Airborne Instrumentation for Astronomy V, 91471G, doi: [10.1117/12.2056417](https://doi.org/10.1117/12.2056417)

- Maldonado, J., Micela, G., Baratella, M., et al. 2020, A&A, 644, A68, doi: [10.1051/0004-6361/202039478](https://doi.org/10.1051/0004-6361/202039478)
- Mankovich, C. R., & Fuller, J. 2021, Nature Astronomy, 5, 1103, doi: [10.1038/s41550-021-01448-3](https://doi.org/10.1038/s41550-021-01448-3)
- Marley, M. S., Ackerman, A. S., Cuzzi, J. N., & Kitzmann, D. 2013, Clouds and Hazes in Exoplanet Atmospheres, ed. S. J. Mackwell, A. A. Simon-Miller, J. W. Harder, & M. A. Bullock, 367–392, doi: [10.2458/azu_uapress_9780816530595-ch015](https://doi.org/10.2458/azu_uapress_9780816530595-ch015)
- Marzari, F., & Thebault, P. 2019, Galaxies, 7, 84, doi: [10.3390/galaxies7040084](https://doi.org/10.3390/galaxies7040084)
- Masci, F. J., Laher, R. R., Rusholme, B., et al. 2019, PASP, 131, 018003, doi: [10.1088/1538-3873/aae8ac](https://doi.org/10.1088/1538-3873/aae8ac)
- Mayor, M., Marmier, M., Lovis, C., et al. 2011, arXiv e-prints, arXiv:1109.2497. <https://arxiv.org/abs/1109.2497>
- McKinney, W. 2010, in Proceedings of the 9th Python in Science Conference, ed. S. van der Walt & J. Millman, 51 – 56
- Metcalf, A., Anderson, T., Bender, C., et al. 2019, Optica, 6, 233, doi: [10.1364/OPTICA.6.000233](https://doi.org/10.1364/OPTICA.6.000233)
- Miller, N., & Fortney, J. J. 2011, ApJL, 736, L29, doi: [10.1088/2041-8205/736/2/L29](https://doi.org/10.1088/2041-8205/736/2/L29)
- Mordasini, C., Alibert, Y., Benz, W., Klahr, H., & Henning, T. 2012, A&A, 541, A97, doi: [10.1051/0004-6361/201117350](https://doi.org/10.1051/0004-6361/201117350)
- Moses, J. I., Visscher, C., Fortney, J. J., et al. 2011, ApJ, 737, 15, doi: [10.1088/0004-637X/737/1/15](https://doi.org/10.1088/0004-637X/737/1/15)
- Mugrauer, M., & Neuhäuser, R. 2005, MNRAS, 361, L15, doi: [10.1111/j.1745-3933.2005.00055.x](https://doi.org/10.1111/j.1745-3933.2005.00055.x)
- Mustill, A. J., Davies, M. B., & Johansen, A. 2015, ApJ, 808, 14, doi: [10.1088/0004-637X/808/1/14](https://doi.org/10.1088/0004-637X/808/1/14)
- Naoz, S., Farr, W. M., Lithwick, Y., Rasio, F. A., & Teyssandier, J. 2011, Nature, 473, 187, doi: [10.1038/nature10076](https://doi.org/10.1038/nature10076)
- Neves, V., Bonfils, X., Santos, N. C., et al. 2013, A&A, 551, A36, doi: [10.1051/0004-6361/201220574](https://doi.org/10.1051/0004-6361/201220574)
- Newton, E. R., Irwin, J., Charbonneau, D., et al. 2016, ApJ, 821, 93, doi: [10.3847/0004-637X/821/2/93](https://doi.org/10.3847/0004-637X/821/2/93)
- Ngo, H., Knutson, H. A., Hinkley, S., et al. 2015, ApJ, 800, 138, doi: [10.1088/0004-637X/800/2/138](https://doi.org/10.1088/0004-637X/800/2/138)
- . 2016, ApJ, 827, 8, doi: [10.3847/0004-637X/827/1/8](https://doi.org/10.3847/0004-637X/827/1/8)
- Ninan, J. P., Bender, C. F., Mahadevan, S., et al. 2018, in Society of Photo-Optical Instrumentation Engineers (SPIE) Conference Series, Vol. 10709, Proc. SPIE, 107092U, doi: [10.1117/12.2312787](https://doi.org/10.1117/12.2312787)
- Nordhaus, J., & Spiegel, D. S. 2013, MNRAS, 432, 500, doi: [10.1093/mnras/stt569](https://doi.org/10.1093/mnras/stt569)
- Nordhaus, J., Spiegel, D. S., Ibgui, L., Goodman, J., & Burrows, A. 2010, MNRAS, 408, 631, doi: [10.1111/j.1365-2966.2010.17155.x](https://doi.org/10.1111/j.1365-2966.2010.17155.x)
- Obermeier, C., Koppenhoefer, J., Saglia, R. P., et al. 2016, A&A, 587, A49, doi: [10.1051/0004-6361/201527633](https://doi.org/10.1051/0004-6361/201527633)
- Osborn, A., & Bayliss, D. 2020, MNRAS, 491, 4481, doi: [10.1093/mnras/stz3207](https://doi.org/10.1093/mnras/stz3207)
- Paczynski, B. 1971, ARA&A, 9, 183, doi: [10.1146/annurev.aa.09.090171.001151](https://doi.org/10.1146/annurev.aa.09.090171.001151)
- Paczynski, B. 1976, in Structure and Evolution of Close Binary Systems, ed. P. Eggleton, S. Mitton, & J. Whelan, Vol. 73, 75
- Penoyre, Z., Belokurov, V., Wyn Evans, N., Everall, A., & Koposov, S. E. 2020, MNRAS, 495, 321, doi: [10.1093/mnras/staa1148](https://doi.org/10.1093/mnras/staa1148)
- Petigura, E. A., Marcy, G. W., Winn, J. N., et al. 2018, AJ, 155, 89, doi: [10.3847/1538-3881/aaa54c](https://doi.org/10.3847/1538-3881/aaa54c)
- Petrovich, C. 2015a, ApJ, 799, 27, doi: [10.1088/0004-637X/799/1/27](https://doi.org/10.1088/0004-637X/799/1/27)
- . 2015b, ApJ, 805, 75, doi: [10.1088/0004-637X/805/1/75](https://doi.org/10.1088/0004-637X/805/1/75)
- Pineda, J. S., Youngblood, A., & France, K. 2021, ApJ, 911, 111, doi: [10.3847/1538-4357/abe8d7](https://doi.org/10.3847/1538-4357/abe8d7)
- Pollack, J. B., Hubickyj, O., Bodenheimer, P., et al. 1996, Icarus, 124, 62, doi: [10.1006/icar.1996.0190](https://doi.org/10.1006/icar.1996.0190)
- Price-Whelan, A. M., Hogg, D. W., Foreman-Mackey, D., & Rix, H.-W. 2017, ApJ, 837, 20, doi: [10.3847/1538-4357/aa5e50](https://doi.org/10.3847/1538-4357/aa5e50)
- Queloz, D., Mayor, M., Weber, L., et al. 2000, A&A, 354, 99
- Rasio, F. A., & Ford, E. B. 1996, Science, 274, 954, doi: [10.1126/science.274.5289.954](https://doi.org/10.1126/science.274.5289.954)
- Reinhold, T., & Hekker, S. 2020, A&A, 635, A43, doi: [10.1051/0004-6361/201936887](https://doi.org/10.1051/0004-6361/201936887)
- Ricker, G. R., Winn, J. N., Vanderspek, R., et al. 2015, Journal of Astronomical Telescopes, Instruments, and Systems, 1, 014003, doi: [10.1117/1.JATIS.1.1.014003](https://doi.org/10.1117/1.JATIS.1.1.014003)

- Robertson, P., Anderson, T., Stefansson, G., et al. 2019, Journal of Astronomical Telescopes, Instruments, and Systems, 5, 015003, doi: [10.1117/1.JATIS.5.1.015003](https://doi.org/10.1117/1.JATIS.5.1.015003)
- Sabotta, S., Schlecker, M., Chaturvedi, P., et al. 2021, A&A, 653, A114, doi: [10.1051/0004-6361/202140968](https://doi.org/10.1051/0004-6361/202140968)
- Schönrich, R., Binney, J., & Dehnen, W. 2010, MNRAS, 403, 1829, doi: [10.1111/j.1365-2966.2010.16253.x](https://doi.org/10.1111/j.1365-2966.2010.16253.x)
- Schwab, C., Rakich, A., Gong, Q., et al. 2016, Society of Photo-Optical Instrumentation Engineers (SPIE) Conference Series, Vol. 9908, Design of NEID, an extreme precision Doppler spectrograph for WIYN, 99087H, doi: [10.1117/12.2234411](https://doi.org/10.1117/12.2234411)
- Scott, N. J., Howell, S. B., Horch, E. P., & Everett, M. E. 2018, PASP, 130, 054502, doi: [10.1088/1538-3873/aab484](https://doi.org/10.1088/1538-3873/aab484)
- Seager, S., & Mallén-Ornelas, G. 2003, ApJ, 585, 1038, doi: [10.1086/346105](https://doi.org/10.1086/346105)
- Shetrone, M., Cornell, M. E., Fowler, J. R., et al. 2007, PASP, 119, 556, doi: [10.1086/519291](https://doi.org/10.1086/519291)
- Sing, D. K. 2018, arXiv e-prints, arXiv:1804.07357. <https://arxiv.org/abs/1804.07357>
- Sing, D. K., Fortney, J. J., Nikolov, N., et al. 2016, Nature, 529, 59, doi: [10.1038/nature16068](https://doi.org/10.1038/nature16068)
- Speagle, J. S. 2020, MNRAS, 493, 3132, doi: [10.1093/mnras/staa278](https://doi.org/10.1093/mnras/staa278)
- Stassun, K. G., & Torres, G. 2021, ApJL, 907, L33, doi: [10.3847/2041-8213/abdaad](https://doi.org/10.3847/2041-8213/abdaad)
- Stassun, K. G., Oelkers, R. J., Paegert, M., et al. 2019, AJ, 158, 138, doi: [10.3847/1538-3881/ab3467](https://doi.org/10.3847/1538-3881/ab3467)
- Stefánsson, G., Hearty, F., Robertson, P., et al. 2016, ApJ, 833, 175, doi: [10.3847/1538-4357/833/2/175](https://doi.org/10.3847/1538-4357/833/2/175)
- Stefánsson, G., Mahadevan, S., Hebb, L., et al. 2017, ApJ, 848, 9, doi: [10.3847/1538-4357/aa88aa](https://doi.org/10.3847/1538-4357/aa88aa)
- Stefánsson, G., Cañas, C., Wisniewski, J., et al. 2020, AJ, 159, 100, doi: [10.3847/1538-3881/ab5f15](https://doi.org/10.3847/1538-3881/ab5f15)
- Stefánsson, G., Mahadevan, S., Petrovich, C., et al. 2021, arXiv e-prints, arXiv:2111.01295. <https://arxiv.org/abs/2111.01295>
- Steffen, J. H., Ragozzine, D., Fabrycky, D. C., et al. 2012, Proceedings of the National Academy of Science, 109, 7982, doi: [10.1073/pnas.1120970109](https://doi.org/10.1073/pnas.1120970109)
- Sudarsky, D., Burrows, A., & Hubeny, I. 2003, ApJ, 588, 1121, doi: [10.1086/374331](https://doi.org/10.1086/374331)
- Tenenbaum, P., & Jenkins, J. 2018, TESS Science Data Products Description Document, Tech. rep. <https://ntrs.nasa.gov/archive/nasa/casi/ntrs.nasa.gov/20180007935.pdf>
- Thorngren, D. P., & Fortney, J. J. 2018, AJ, 155, 214, doi: [10.3847/1538-3881/aaba13](https://doi.org/10.3847/1538-3881/aaba13)
- Thorngren, D. P., Fortney, J. J., Lopez, E. D., Berger, T. A., & Huber, D. 2021, ApJL, 909, L16, doi: [10.3847/2041-8213/abe86d](https://doi.org/10.3847/2041-8213/abe86d)
- Triaud, A. H. M. J. 2018, The Rossiter-McLaughlin Effect in Exoplanet Research, 2, doi: [10.1007/978-3-319-55333-7_2](https://doi.org/10.1007/978-3-319-55333-7_2)
- van der Walt, S., Colbert, S. C., & Varoquaux, G. 2011, Computing in Science and Engineering, 13, 22, doi: [10.1109/MCSE.2011.37](https://doi.org/10.1109/MCSE.2011.37)
- VanderPlas, J. T. 2018, ApJS, 236, 16, doi: [10.3847/1538-4365/aab766](https://doi.org/10.3847/1538-4365/aab766)
- Veras, D. 2016, Royal Society Open Science, 3, 150571, doi: [10.1098/rsos.150571](https://doi.org/10.1098/rsos.150571)
- Vick, M., Lai, D., & Anderson, K. R. 2019, MNRAS, 484, 5645, doi: [10.1093/mnras/stz354](https://doi.org/10.1093/mnras/stz354)
- Virtanen, P., Gommers, R., Oliphant, T. E., et al. 2020, Nature Methods, 17, 261, doi: [10.1038/s41592-019-0686-2](https://doi.org/10.1038/s41592-019-0686-2)
- Wahl, S. M., Hubbard, W. B., Militzer, B., et al. 2017, Geophys. Res. Lett., 44, 4649, doi: [10.1002/2017GL073160](https://doi.org/10.1002/2017GL073160)
- Wang, J., Fischer, D. A., Xie, J.-W., & Ciardi, D. R. 2014, ApJ, 791, 111, doi: [10.1088/0004-637X/791/2/111](https://doi.org/10.1088/0004-637X/791/2/111)
- Wang, X.-Y., Rice, M., Wang, S., et al. 2021a, arXiv e-prints, arXiv:2110.08832. <https://arxiv.org/abs/2110.08832>
- Wang, X.-Y., Wang, Y.-H., Wang, S., et al. 2021b, ApJS, 255, 15, doi: [10.3847/1538-4365/ac0835](https://doi.org/10.3847/1538-4365/ac0835)
- Weidenschilling, S. J., & Marzari, F. 1996, Nature, 384, 619, doi: [10.1038/384619a0](https://doi.org/10.1038/384619a0)
- Winn, J. N. 2010, arXiv e-prints, arXiv:1001.2010. <https://arxiv.org/abs/1001.2010>
- Winn, J. N., & Fabrycky, D. C. 2015, ARA&A, 53, 409, doi: [10.1146/annurev-astro-082214-122246](https://doi.org/10.1146/annurev-astro-082214-122246)
- Wright, E. L., Eisenhardt, P. R. M., Mainzer, A. K., et al. 2010, AJ, 140, 1868, doi: [10.1088/0004-6256/140/6/1868](https://doi.org/10.1088/0004-6256/140/6/1868)
- Wright, J. T., & Eastman, J. D. 2014, PASP, 126, 838, doi: [10.1086/678541](https://doi.org/10.1086/678541)

- Wright, J. T., Marcy, G. W., Howard, A. W., et al. 2012, *ApJ*, 753, 160, doi: [10.1088/0004-637X/753/2/160](https://doi.org/10.1088/0004-637X/753/2/160)
- Wu, Y., & Murray, N. 2003, *ApJ*, 589, 605, doi: [10.1086/374598](https://doi.org/10.1086/374598)
- Xiang, M. S., Liu, X. W., Yuan, H. B., et al. 2017, *MNRAS*, 467, 1890, doi: [10.1093/mnras/stx129](https://doi.org/10.1093/mnras/stx129)
- Yee, S. W., Petigura, E. A., & von Braun, K. 2017, *ApJ*, 836, 77, doi: [10.3847/1538-4357/836/1/77](https://doi.org/10.3847/1538-4357/836/1/77)
- Yuan, H. B., Liu, X. W., Huo, Z. Y., et al. 2015, *MNRAS*, 448, 855, doi: [10.1093/mnras/stu2723](https://doi.org/10.1093/mnras/stu2723)
- Zechmeister, M., & Kürster, M. 2009, *A&A*, 496, 577, doi: [10.1051/0004-6361:200811296](https://doi.org/10.1051/0004-6361:200811296)
- Zechmeister, M., Reiners, A., Amado, P. J., et al. 2018, *A&A*, 609, A12, doi: [10.1051/0004-6361/201731483](https://doi.org/10.1051/0004-6361/201731483)
- Zhong, J., Li, J., Carlin, J. L., et al. 2019, *ApJS*, 244, 8, doi: [10.3847/1538-4365/ab3859](https://doi.org/10.3847/1538-4365/ab3859)
- Zhong, J., Lépine, S., Hou, J., et al. 2015, *AJ*, 150, 42, doi: [10.1088/0004-6256/150/2/42](https://doi.org/10.1088/0004-6256/150/2/42)
- Zhou, G., Huang, C. X., Bakos, G. Á., et al. 2019, *AJ*, 158, 141, doi: [10.3847/1538-3881/ab36b5](https://doi.org/10.3847/1538-3881/ab36b5)
- Zhu, W., Dai, F., & Masuda, K. 2018, *Research Notes of the American Astronomical Society*, 2, 160, doi: [10.3847/2515-5172/aade53](https://doi.org/10.3847/2515-5172/aade53)
- Zhu, W., & Dong, S. 2021, *ARA&A*, 59, doi: [10.1146/annurev-astro-112420-020055](https://doi.org/10.1146/annurev-astro-112420-020055)